

Treball de Fi de Màster

Master's in Renewable Energy
Hydrodynamic analysis of semi-
submersible floating platform combined
with wave energy converters

MEMÒRIA

Author: Shreya Tushar Chavan
Director: Oriol Gomis-Bellmunt
Call: 2nd October 2024



Escola Tècnica Superior d'Enginyeria

Industrial de Barcelona



Abstract

This study investigates the performance of a hybrid floating platform equipped with Point Absorber Wave Energy Converters (PAWECs). It provides an in-depth analysis of the platform's dynamics, WEC efficiency, and overall power production capabilities. A thorough literature review on floating offshore wind turbines, wave energy converters, and hybrid systems forms the theoretical basis. Metocean data from a selected site in the Irish Sea is analyzed to identify key factors affecting performance. A comprehensive design of the Hybrid Floating Wind-Wave Platform (HFWWP) is developed using SolidWorks, and a hydrodynamic analysis is performed using Ansys AQWA to model the platform's response to waves. These simulations are validated against experimental data. Time-domain analysis using WEC-Sim is carried out to simulate power generation under varying wave conditions.

Key findings include a significant reduction in pitch motion with the integration of WECs, which improves platform stability. The Response Amplitude Operator (RAO) results showed that the addition of WECs dampened surge and pitch motions, enhancing overall platform stability. Additionally, the optimal Power Take-Off (PTO) damping coefficient was identified, maximizing energy production across different sea states. The research concludes that hybrid floating platforms hold strong potential as a sustainable and efficient renewable energy solution.

Table of Contents

Abstract.....	3
Abbreviations.....	7
List of Figures.....	8
List of Tables	9
<u>1.</u> Introduction.....	11
1.1 Motivation.....	11
1.2 Scope.....	12
1.3 Objectives	13
<u>2.</u> Theoretical background	14
2.1 Theoretical foundation	14
2.1.1 Wave mechanics and wave energy.....	14
2.1.2 Potential flow theory and Linear (Airy) wave theory.....	15
2.1.3 Wave energy.....	17
2.1.4 Hydrodynamic diffraction.....	19
2.1.5 Boundary Element Method (BEM).....	20
2.1.6 Numerical modelling.....	20
2.1.7 Equation of motion	20
2.2 Background and state of the matter.....	21
2.2.1 Offshore Renewable Energy	21
2.2.2 Floating platforms.....	23
2.2.3 WECs.....	25
2.2.4 HWWFP	26
<u>3.</u> Methodology	27
3.1 Reference site	27
3.2 Design parameters	30
3.2.1 Orientation and coordinate system.....	30
3.2.2 SSP.....	31
3.2.3 WECs.....	32
3.2.4 HWWFP	33
3.3 System properties.....	34
3.4 Power generation	36

3.4.1 BEMIO	37
3.4.2 Simulink model.....	37
3.4.3 PTO	38
3.4.4 Inputs.....	39
<u>4.</u> Results and discussion	41
4.1 Hydrodynamic diffraction results	41
4.1.1 Validation for SSP	41
4.1.2 RAO	42
4.1.3 Hydrodynamic coefficients and forces	45
4.1.3.2 Hydrodynamic diffraction	47
4.2 Time domain analysis	49
<u>5.</u> Conclusion.....	52
<u>6.</u> Limitations and recommended future works.....	53
Acknowledgements	55
References	56
Appendix A	60

Abbreviations

BEM – Boundary Element Method

CAD – Computer-Aided Design

DOF – Degree of Freedom

EU – European Union

GW – Giga Watt

HD – Hydrodynamic Diffraction

HFWWP – Hybrid Floating Wind and Wave Platform

JPD – Joint Probability Distribution

MW – Mega Watt

PAWEC – Point Absorber Wave Energy Converters

PTO – Power Take Off

RAO – Response Amplitude Operator

SS – Sea State

SSP – Semi-Submersible Platform

SW – SolidWorks

SWL – Sea Water Level

SWL – Surface Water Level

WEC – Wave Energy Converter

Wec-SIM – Wave energy converter SIMulator

List of Figures

Figure 1. Simple representation of ocean wave [17]	15
Figure 2. Governing equations for WEC hydrodynamic modelling [19]	15
Figure 3. Relative amounts of energy as a function of wave period in ocean waves[17] .	19
Figure 4. Hydrodynamics of a semi-submerged body	21
Figure 5. Global distribution of ocean energy activity [24]	23
Figure 6. Classification of Offshore Wind Structures [38]	24
Figure 7. DeepCwind floating platform.....	25
Figure 8. Classification of PAWECs[57]	26
Figure 9. Site location.....	28
Figure 10. Joint probability distribution between Significant wave height and Peak period.	29
Figure 11. Coordinate system.....	31
Figure 12. Structures of SSP	31
Figure 13. WEC dimensions	33
Figure 14. HWWFP layout.....	34
Figure 15. Meshed HWWFP.....	36
Figure 16. Optimal PTO damping coefficient for WECs	39
Figure 17. Natural modes for SSP	42
Figure 18. Surge RAO for SSP and HWWFP	43
Figure 19. Heave RAO for SSP and HWWFP.....	44
Figure 20. Pitch RAO for SSP and HWWFP	44
Figure 21. Surge component of radiation damping for SSP and HWWFP.....	46
Figure 22. Heave component of radiation damping for SSP and HWWFP	46
Figure 23. Pitch component of radiation damping for SSP and HWWFP	47
Figure 24. Surge component of hydrodynamic diffraction forces for HWWFP and SSP ..	48
Figure 25. Heave component of hydrodynamic diffraction forces for HWWFP and SSP .	48
Figure 26. Pitch component of hydrodynamic diffraction forces for HWWFP and SSP....	49
Figure 27. Forces and moment acting on SSP for different SS	50
Figure 28. SSP surge, heave and pitch for different SS	50
Figure 29. Power generation from WEC 1 for different SS.....	51
Figure 30. Power generated by each WEC for SS3.....	52
Figure 31. HWWFP Simulink model.....	61

List of Tables

Table 1. Design parameters for SSP.....	32
Table 2. Design parameters for WEC	32
Table 3. Design parameters for HWWFP	33
Table 4. Properties of SSP and WEC.....	35
Table 5. Mesh details.....	35
Table 6. Simulation parameters for HD	35
Table 7. Input parameters for Wec-SIM	40
Table 8. Sea states definition	40
Table 9. Comparison of AQWA with experimental results of 3 DOF motion natural periods	42



1. Introduction

This section outlines the motivation and objectives of the study, focusing on the pressing need to transition from fossil fuels to renewable energy sources like offshore wind and wave energy. It sets the context for exploring a hybrid floating platform that combines wind and wave energy technologies, presenting an innovative solution for efficient renewable power generation. The key aspects covered include the study's purpose, scope, and intended contributions to the field of renewable energy systems.

1.1 Motivation

The past few decades have shown the adverse effects of climate change caused by the heavy reliance on fossil fuels. This is driving the shift towards renewable energy and has already led to astonishing growth in the said sector. The wind energy sector has followed this trend. The floating offshore wind energy sector has seen significant growth over the past two decades [1]. This growth is driven by technological advancements, increasing demand for renewable energy, and the need to access deeper waters where traditional fixed-bottom turbines are not feasible. The global operational capacity of floating offshore wind will reach approximately 270 MW by 2023. The pipeline of new projects is substantial, with a projected 244 GW of new floating wind projects [2].

In recent years, the wave energy sector has also seen significant growth. It is recognised as a source of sustainable power generation and has a huge potential for power generation, but it still faces multiple challenges such as technological, economic, environmental and regulatory [3-5]. Despite the research done on wave energy devices, which started in the early 1970's by Stephen Salter [6], the sector still lags due to the multiple reasons. There have been some significant advancements in wave energy technology, yet it has not yet been widely adopted for commercial power generation due to its relatively low power output and high installation costs. These factors make the cost of electricity from wave energy less competitive compared to other renewable sources. Reducing its costs is crucial to make wave energy commercially viable.

While offshore wind farms have become more common, many are built on fixed structures in shallow waters. Recently, floating wind farms have been introduced, and are still developing, but studies on hybrid concepts like wind-wave and wind-solar show promise in reducing costs and increasing energy yield per unit area of ocean [7-9]. By integrating wave energy converters (WECs) into existing offshore wind farm infrastructure, such as substructures, power grids, and moorings, we can potentially make wave energy more economical. This integration not only reduces costs but also increases the overall power output of the combined wind-wave energy system [10-12]. Combining wave energy converters with a floating platform can help balance the fluctuating nature of wind energy,

resulting in a more stable and reliable power supply. WECs can also stabilize the platform, improving its safety and overall structural integrity [13, 14].

This gives the understanding that the floating offshore energy sector offers a promising avenue for sustainable and renewable energy generation. By harnessing the power of wind and waves in offshore environments, these projects can contribute significantly to addressing climate change and reducing reliance on fossil fuels. With vast ocean resources and advancements in technology, floating offshore energy has the potential to create new economic opportunities, enhance energy security, and provide a more stable and reliable power supply. As the world transitions towards a low-carbon future, investing in and developing floating offshore energy projects can play a vital role in shaping a sustainable and resilient energy landscape. These positive factors are the main motivation to conduct the study on hybrid floating offshore wind platforms.

1.2 Scope

This thesis aims to explore the technical feasibility and performance of a hybrid floating wind and wave platform (HFWWP) by combining a semi-submersible platform (SSP) with point absorber wave energy converters (PAWECs). The primary focus is on analysing the hydrodynamic interaction between the platform and WECs, their individual motion responses, and the overall energy production capabilities.

Key Areas of Investigation:

Hydrodynamic Stability: The study will investigate the stability of the SSP and PAWECs under various wave conditions, for a given location. The goal is to evaluate that the platform remains stable and that the WECs can efficiently convert wave energy without compromising the overall system's integrity.

Energy Production: The thesis will evaluate the power output from the PAWECs and analyse how their performance is influenced by the platform's motion and wave conditions.

System Integration: The study will explore the interaction between the SSP and PAWECs and assess how their combined operation affects the overall system's efficiency and performance.

This thesis will employ a simulation-based approach to investigate the performance of a HFWWP. The methodology involves selecting an existing, validated design for a DeepCwind floating wind system [15] as the basis for SSP. Additionally, PAWECs will be designed, based on the studies conducted on WECs. To analyse the platform's performance under realistic conditions, the study will focus on a specific location in the Irish Sea, 100 kilometres off the coast of Ireland.

Wave energy converter SIMulator (Wec-SIM) [16], a specialized software for modelling wave energy converters, will be used to create a detailed simulation model of the HFWWP. This model will incorporate the SSP, PAWECs, and the surrounding environmental conditions. By subjecting the simulation model to various wave scenarios, including different wave heights, periods, and directions, the study will assess the platform's and WECs' performance under a range of conditions. Key metrics, such as platform pitch, heave, and surge, as well as WEC power output and system efficiency, will be analysed to evaluate the simulation results. This will provide insights into the platform's motion response, the PAWECs' power production, and the overall system's performance.

While this thesis provides a valuable analysis of the HFWWP, it has certain limitations. The primary focus of the study is on the wave energy component, with the wind turbine included for representation purposes only. This limits the scope of the analysis to the wave energy aspect of the HFWWP. Additionally, the thesis does not include an economic evaluation, which is crucial for assessing the commercial viability of such a system. Future research could delve into these economic aspects.

Furthermore, the study relies solely on simulations and does not involve physical experiments. While simulations provide valuable insights, physical modelling can validate the simulation results and provide additional data on the system's behaviour.

1.3 Objectives

The primary objective of this research is to investigate the performance of a hybrid floating platform equipped with PAWECs. This will involve a comprehensive analysis of the platform's dynamics, WEC efficiency, and overall power production capabilities.

Specific objectives include:

- Conduct a comprehensive literature review on floating offshore wind turbines, wave energy converters, and hybrid systems. This will include an in-depth exploration of theoretical foundations.
- Analyse metocean data for the selected site to identify key parameters that will influence the platform's and WECs' performance.
- Develop a detailed computer-aided design (CAD) model of the HFWWP using SolidWorks to visualize the physical configuration and dimensions.
- Perform a hydrodynamic analysis using Ansys AQWA to determine the platform's response to waves. This will involve a frequency domain analysis to obtain hydrodynamic diffraction coefficients.
- Validate the hydrodynamic data by comparing simulation results with experimental data from existing studies or physical experiments.

- Evaluate the time domain response of the hybrid system, using Wec-SIM, to simulate its behaviour under various wave conditions and assess its power production potential.

2. Theoretical background

In this section, the fundamental concepts that form the basis of the study are discussed, including wave mechanics, potential flow theory, and wave energy conversion principles. It also presents a review of existing technologies for offshore renewable energy, particularly focusing on floating platforms and Wave Energy Converters (WECs). The section concludes with a discussion of the theoretical framework guiding the design and analysis of the hybrid wind-wave platform.

2.1 Theoretical foundation

2.1.1 Wave mechanics and wave energy

Ocean wave mechanics is the study of the physical processes that govern the generation, propagation, and interaction of waves on the surface of the ocean. This field is crucial for understanding coastal processes, designing marine structures, and harnessing wave energy. Waves are primarily generated by wind blowing over the surface of the ocean. The energy transfer from wind to water creates waves, which can travel vast distances. Once generated, waves propagate across the ocean surface. The speed and direction of wave propagation depend on factors such as wave period, wavelength, wave height and water depth as seen in Figure 1. The wave height H is the vertical distance between the crest and the trough of the wave and equals twice the amplitude a for a sinusoidal variation. The wave period T is the time the wave needs to pass the location, the inverse of which is the frequency f , the number of waves passing a fixed location per unit time. The wavelength L of the surface elevation deformation measured along the direction of wave propagation. η is the elevation of a particle, at free surface water level, at a given point in time and location and this is described as equation (1) [17]. These terms are defining the wave and will be used frequently in the following sections.

$$\eta = a \sin(\omega t - kx) = a \sin S(x, t)$$

(1)

here ω is the angular frequency and k is the wavenumber according to:

$$k = \frac{2\pi}{L}; \quad \omega = 2\pi f = \frac{2\pi}{T}$$

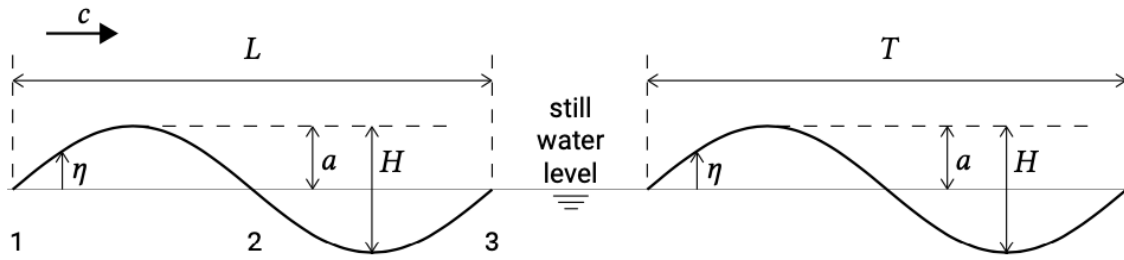


Figure 1. Simple representation of ocean wave [17]

2.1.2 Potential flow theory and Linear (Airy) wave theory

Potential flow theory is a fundamental concept in fluid dynamics that describes the flow of an incompressible, inviscid (frictionless), and irrotational fluid, which are also the key assumptions in this study. These assumptions allow for the use of potential functions to describe the fluid flow and the resulting wave characteristics. While potential flow theory has limitations, especially for nonlinear waves, it remains a valuable tool for understanding and predicting wave behaviour in many practical applications. This theory simplifies the complex Navier-Stokes equations to the Laplace equation, making it easier to analyse fluid flow around objects. It is an important part of the foundations because the numerical models are based on it, as seen in Figure 2. Approaches based on three-dimensional potential theory are employed in Aqwa for hydrodynamic analyses of complex multiple-body systems [18].

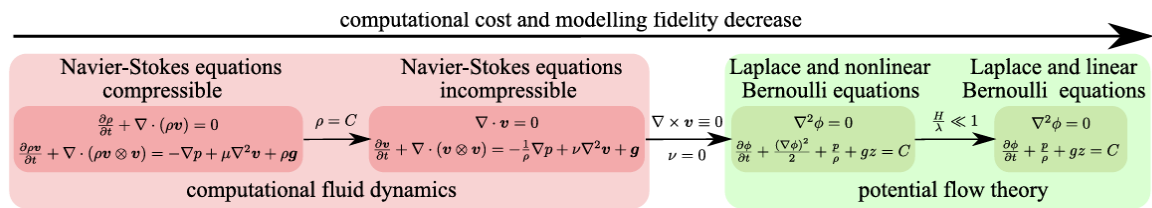


Figure 2. Governing equations for WEC hydrodynamic modelling [19]

Under the said assumptions, the fluid flow can be represented by a scalar function called the velocity potential, Φ . The velocity vector field, V , can be obtained from the gradient of the velocity potential [20]:

$$V = \nabla \Phi \tag{2}$$

The incompressibility condition requires that the divergence of the velocity field is zero:

$$\nabla \cdot V = 0 \quad (3)$$

Where, ∇ is the gradient operator
and $\Phi = \Phi(x, y, z, t)$ is velocity potential function.

By substituting (2) in (3), we arrive at the Laplace equation,

$$\nabla^2 \Phi = 0 \quad (4)$$

The components of velocity in Cartesian coordinates are,

$$u = \frac{\partial \Phi}{\partial x}, v = \frac{\partial \Phi}{\partial y}, w = \frac{\partial \Phi}{\partial z} \quad (5)$$

The velocity must satisfy the conservation of mass equation, which is given by:

$$\frac{\partial u}{\partial x} + \frac{\partial v}{\partial y} + \frac{\partial w}{\partial z} = 0 \quad (6)$$

From equations (4), (5) and (6) we get the Laplace equation in Cartesian coordinates,

$$\nabla^2 \Phi = \frac{\partial^2 \Phi}{\partial x^2} + \frac{\partial^2 \Phi}{\partial y^2} + \frac{\partial^2 \Phi}{\partial z^2} = 0$$

To solve the Laplace equation for a regular wave, as mentioned in equation (1), boundary conditions need to be defined, which describe the wave's characteristics. The kinematic boundary condition represents the motion of the free surface, and states that a fluid particle at the surface should always remain at the water surface [21]. The equation below is a mathematical representation of the kinematic boundary condition of a fluid particle at η :

$$\left\{ \begin{array}{l} \frac{\partial \Phi}{\partial z} = \frac{\partial \eta}{\partial t} \text{ at } z = 0 \end{array} \right.$$

$$\left\{ \begin{array}{l} \frac{\partial \Phi}{\partial z} = 0 \text{ at } z = -d \end{array} \right.$$

Where $-d$ indicates a water depth below the surface water level.

In addition to the kinematic boundary condition, the water surface must also satisfy a dynamic boundary condition. This means that the pressure on the surface of the water must be the same as the pressure of the air above it. This condition is based on Bernoulli's equation, which deals with the forces acting on the water surface. The momentum balance equation, which is based on Newton's second law of motion, describes the relationship between the forces acting on the water surface and its acceleration.

$$\frac{\partial(\rho u)}{\partial t} + \frac{\partial u(\rho u)}{\partial x} + \frac{\partial v(\rho u)}{\partial y} + \frac{\partial w(\rho u)}{\partial z} = F_x$$

Ignoring non-linear terms and simplifying yields the linearized Bernoulli equation for unsteady flow

$$\frac{\partial \phi}{\partial t} + \frac{p}{\rho} + gz = 0$$

In terms of velocity potential, the linearized Bernoulli equation for unsteady flow can be rewritten as

$$\frac{\partial \phi}{\partial t} + g\eta = 0$$

Linear wave theory is the simplest approach to solving the equation for waves. It's a basic approximation of the velocity field. In deep water, linear wave theory assumes that the water depth is much larger than the wavelength. This means that when at the water's surface ($z = 0$), the kinematic and dynamic boundary conditions can be simplified.

$$\frac{\partial \phi}{\partial z} - \frac{\partial \eta}{\partial t} = 0$$

2.1.3 Wave energy

Figure 3. shows the wave energy spectrum, which illustrates the distribution of wave energy across different wave periods. The wave energy spectrum typically shows a peak in the gravity wave band, indicating that most of the wave energy is concentrated in waves with periods between 1 second and 30 seconds. The site selected for the analysis in this study, falls between this period range.

In linear wave theory, which assumes small-amplitude waves, the total wave energy can be divided into two components: kinetic energy and potential energy [22]. Kinetic energy is the energy associated with the motion of the water particles. For a wave, the kinetic energy is related to the velocity of the water particles and potential energy is the energy stored in

the wave due to the elevation of the water surface above its mean level. These are given by:

$$E_k = \int_{z=-d}^{z=\eta} \frac{1}{2} \rho (u^2 + w^2) dz = \frac{1}{4} \rho g a^2$$

$$E_p = \int_{z=-d}^{z=\eta} \rho g z dz = \frac{1}{4} \rho g a^2$$

Significant wave height H_s is a statistical measure used to describe the average height of the highest one-third of waves in a wave record. It provides a representative value for the wave conditions in a given area. It is a widely used metric to describe the severity of wave conditions. It provides a clear and concise way to communicate the wave height. It is more commonly used than mean wave height. It is defined as the average height of the highest one third of the waves:

$$H_s = \frac{1}{N/3} \sum_{j=1}^{N/3} H_j$$

Under Linear wave theory [23], the kinetic and potential energy are the same. Thus, by replacing a with H_s , we get the total energy produced by waves:

$$E_T = \frac{1}{16} \rho g H_s^2 \quad (7)$$

The wave power level, P , per width unit in a wave in terms of the significant wave height (H_s) and the energy period (T_e) can be given as follows:

$$P = \frac{\rho g^2 H_s^2 T_e}{64} \quad (8)$$

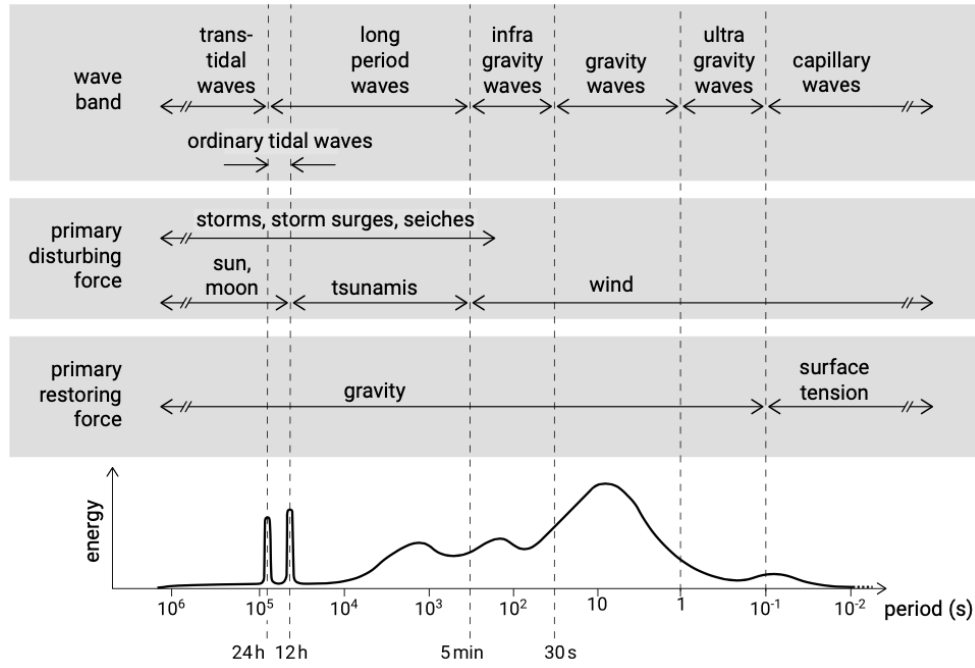


Figure 3. Relative amounts of energy as a function of wave period in ocean waves[17]

2.1.4 Hydrodynamic diffraction

Hydrodynamic diffraction involves the interaction of waves with structures, leading to wave scattering and the generation of forces on the structure. The analysis is based on the theory mentioned in 2.1.2. Hydrodynamic coefficients, including added mass and radiation damping, are calculated to represent the inertia and energy dissipation due to wave-structure interaction. Wave excitation forces and moments are also determined. The added mass and damping are the imaginary and real parts, respectively, of the radiation wave potential, φ_{rk} , and are given by:

$$A_{jk} = \frac{\rho}{\omega} \int_{S_0} \text{Im} [\varphi_{rk}(\vec{X})] n_j dS$$

$$B_{jk} = -\rho \int_{S_0} \text{Re} [\varphi_{rk}(\vec{X})] n_j dS$$

Where, \vec{X} is the space dependent potential term, n_j is the j^{th} unit normal vector of the body surface pointing outwards, and S_0 is the wetted surface of the body in still water. The term $j = (1,6)$ is the notation for the conventional six DOFs. The complete derivation of these terms can be found in [18].

2.1.5 Boundary Element Method (BEM)

The Boundary Element Method (BEM) is extensively used in hydrodynamics to analyse the interaction between fluid and structures, such as ships, offshore platforms, and wave energy converters. BEM reduces a 3D problem to a 2D surface problem by focusing on the boundaries of the domain rather than the entire volume. The method transforms the governing partial differential equations into integral equations over the boundary of the domain. This is particularly useful for problems involving infinite or semi-infinite domains, such as wave propagation. The problem is divided into diffraction and radiation components. The Boundary Element Method (BEM) is used to solve the boundary value problem, with the structure's surface discretized into panels. Hydrodynamic coefficients, including added mass and radiation damping, are calculated to represent the inertia and energy dissipation due to wave-structure interaction. Wave excitation forces and moments are also determined. In ANSYS AQWA, the structure is meshed, and the hydrodynamic diffraction analysis is performed using specific solver settings.

2.1.6 Numerical modelling

Time domain analysis examines how a signal or system's output changes over time, providing direct insights into its dynamic behaviour and transient responses. In contrast, frequency domain analysis transforms time-domain signals into their frequency components, revealing the signal's frequency content and aiding in spectral analysis, resonance identification, and filter design.

For analysing a hybrid wind-wave floating platform, both time domain and frequency domain analyses were essential. Time domain analysis was crucial for observing the platform's dynamic response to time-varying wave conditions. Frequency domain analysis focused on understanding the frequency characteristics of the platform and its interaction with waves. This analysis was particularly useful for identifying resonant frequencies, and stability of the platform. To achieve the best results, a combined approach was used. Starting with frequency domain analysis to identify key resonant frequencies and optimize the design for energy capture, followed by time domain analysis to evaluate the platform's performance under realistic, time-varying wave and wind conditions and to fine-tune control systems.

2.1.7 Equation of motion

The equation of motion for a floating body in hydrodynamics typically involves the balance of forces and moments acting on the body. This equation accounts for the body's inertia, hydrodynamic forces, and external forces such as gravity and buoyancy. The general equation of motion for a floating body is given by:



$$m\ddot{X} = F_{ext}(t) + F_{md}(t) + F_{rad}(t) + F_{pto}(t) + F_v(t) + F_{me}(t) + F_B(t) + F_m(t) \quad (9)$$

where \ddot{X} is the (translational and rotational) acceleration vector of the device, m is the mass matrix, $F_{ext}(t)$ is the wave excitation force and torque (6-element) vector, $F_{md}(t)$ is the mean drift force and torque vector, $F_{rad}(t)$ is the force and torque vector resulting from wave radiation, $F_{pto}(t)$ is the Power Take Off (PTO) force and torque vector, $F_v(t)$ is the damping force and torque vector, $F_{me}(t)$ is the Morison Element force and torque vector, $F_B(t)$ is the net buoyancy restoring force and torque vector, and $F_m(t)$ is the force and torque vector resulting from the mooring connection.

$F_{ext}(t)$, $F_{rad}(t)$, and $F_B(t)$ are calculated using hydrodynamic coefficients provided by the frequency-domain BEM solver, ANSYS AQWA. How these forces act on an actual floating body can be seen in Figure 4.

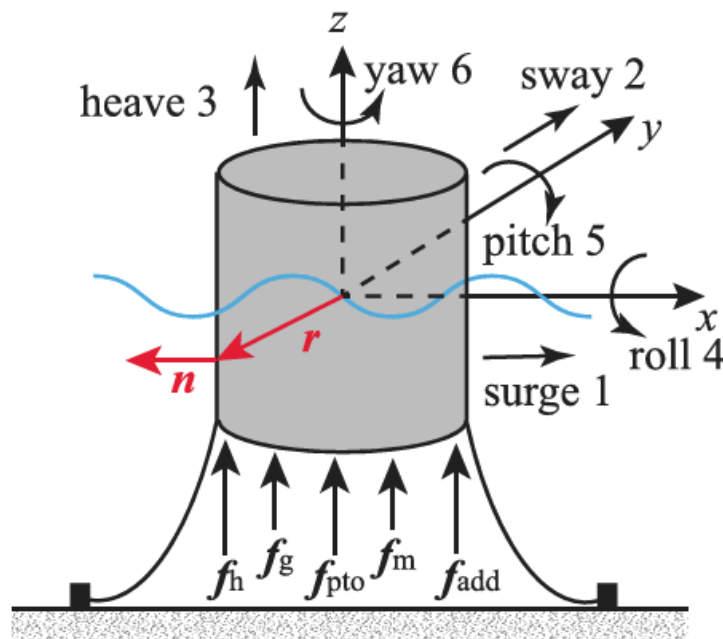


Figure 4. Hydrodynamics of a semi-submerged body

2.2 Background and state of the matter

2.2.1 Offshore Renewable Energy

Offshore renewable energy, such as wind, wave power and tidal, is crucial for reducing carbon emissions and achieving sustainable energy goals. Many countries are leveraging the vast oceans to generate clean energy. Figure 5. highlights the global landscape of ocean energy development, with Europe as a key player and emerging markets showing

increasing interest in this renewable energy source. The majority of ocean energy projects are concentrated in Europe, particularly in the North Sea and Atlantic regions. This reflects the strong focus on renewable energy development and the favourable geographical conditions for ocean energy in these areas [24].

As of 2020, global installed offshore wind capacity exceeded 34 GW, with Europe accounting for over 70% of this capacity. Leading countries in offshore wind deployment include China, Denmark, the UK, and Germany. Amidst the COVID-19 pandemic, governments worldwide have set ambitious targets for offshore wind development, aligning with the Paris Agreement's goal of limiting global temperature rise to 1.5°C [25].

Currently, tidal barrage projects dominate the current market, followed by wave energy, while other ocean technologies remain in research stages. European countries and Australia lead in ocean energy development, with a focus on tidal stream and wave energy. The European Commission aims for at least 1 GW of installed capacity for wave and tidal energy in the EU by 2030 and 40 GW by 2050 [26]. Beyond Europe, countries like China, Japan, and the Republic of Korea are emerging as key players in ocean energy innovation [27].

Since this study focuses on the site in the Northern Seas, it is worth noting that countries along this corridor, Belgium, Denmark, Germany, Ireland, France, Luxembourg, Netherlands, and Sweden have set a non-binding agreement for priority offshore grid corridor Northern Seas offshore grids (NSOG), and Ireland aims to increase generation to 13 GW by 2040 [28].

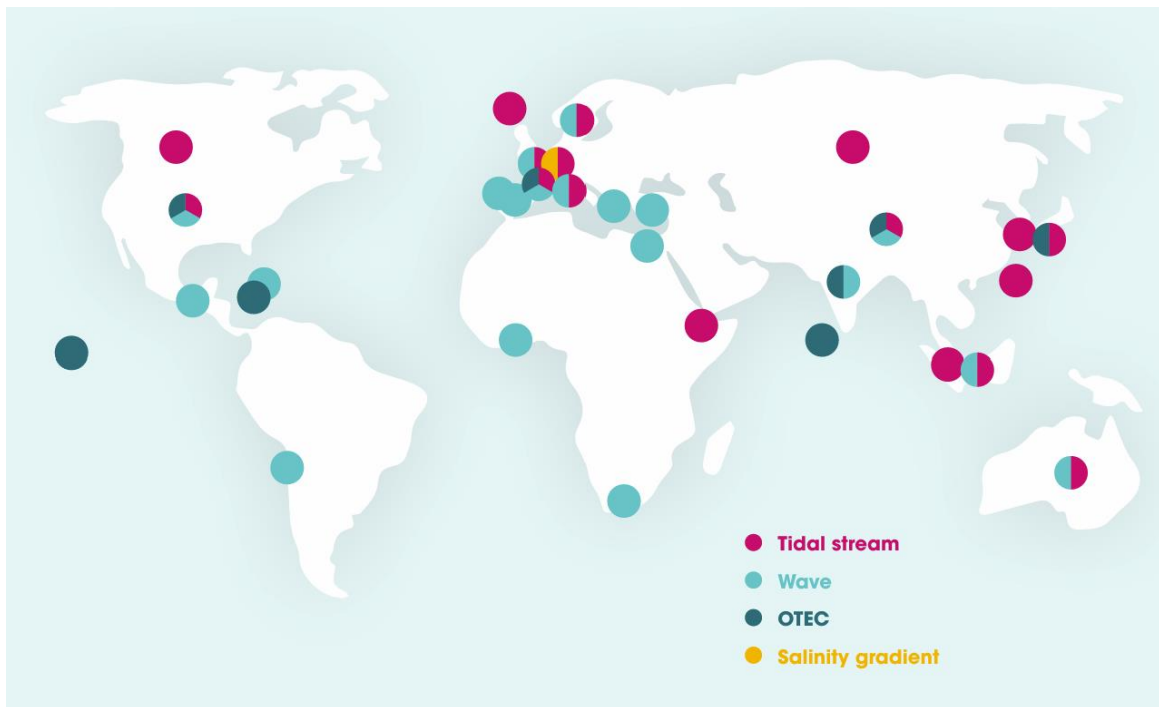


Figure 5. Global distribution of ocean energy activity [24]

2.2.2 Floating platforms

The transition from onshore to offshore wind energy started with the commercial installation of a wind farm, Vindeby, built by Denmark in 1991, with a total capacity of 5MW [29]. Since then, the offshore wind industry has evolved tremendously and has been embraced due to its potential benefits over onshore wind. Offshore wind farms have several advantages over onshore wind farms. They have less environmental impact, allowing for larger turbines and faster spinning blades. This leads to higher electricity production and lower costs. Offshore wind farms can produce up to 50% more electricity than onshore farms because of stronger and more consistent winds. While land-based wind farms are limited in size, offshore farms can be much larger, with capacities exceeding 100 MW. This shift towards offshore wind has led to advancements in wind energy technology [30-32].

Within offshore wind turbines, there are two main types: fixed-support and floating as seen in Figure 6. Fixed-support turbines can be either monopiles or jackets. Monopiles are single tower-like structures embedded in the seabed, while jackets have a lattice structure with three or four legs. Fixed-support turbines are limited to a maximum seabed depth of 60 meters, which is a problem because most of the world's offshore wind energy is found in deeper waters. These turbines are also limited in size, with the largest rotor diameter currently being 80 meters [33]. Floating wind structures allows the industry to enhance the capacity and efficiency of the offshore wind energy sector. With these benefits in mind, multiple projects have been planned, and deployed, for areas with deeper waters such as

Fukushima FORWARD project in Japan [34, 35], the Hywind project in Scotland demonstrating a spar-type substructure [36] and the WindFloat Atlantic in Portugal using a semi-submersible floating structure[37].

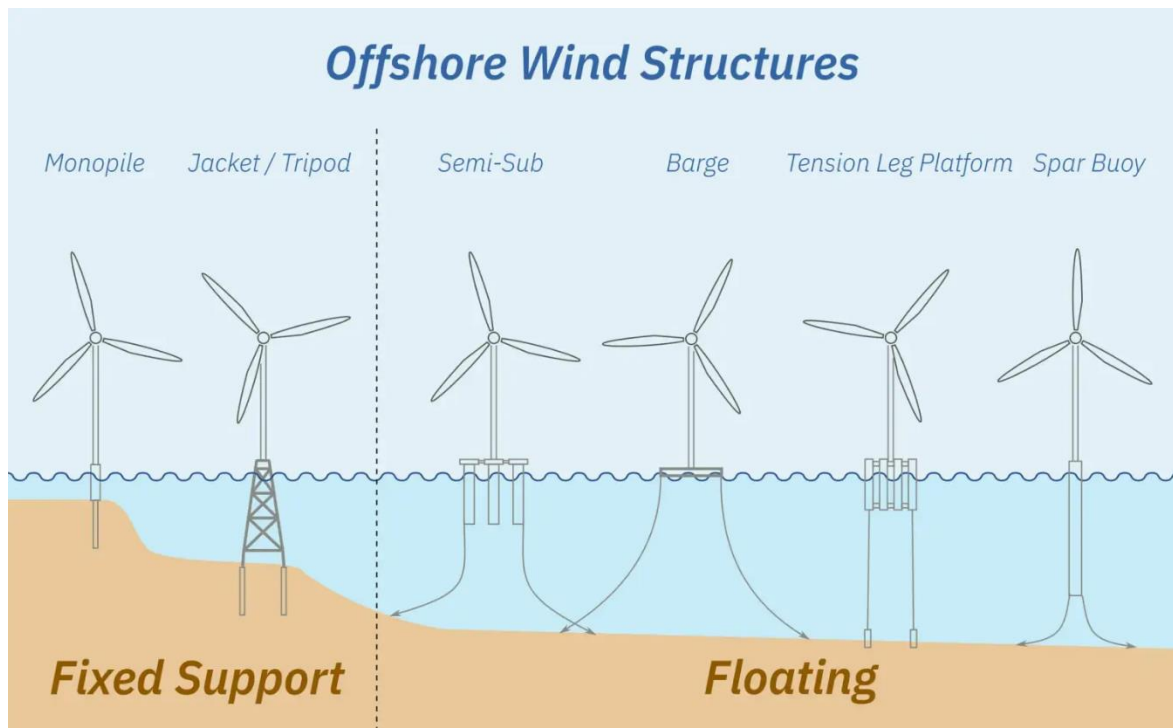


Figure 6. Classification of Offshore Wind Structures [38]

2.2.2.1 SSP

The design principles and technologies developed for oil and gas production in deep waters have been adapted and refined for use in the renewable energy sector. Existing oil rig platforms inspire many of the foundational engineering concepts used for SSPs. Semi-submersible platforms offer several benefits, including the ability to carry heavy loads, function in various water depths, and be moved after they are no longer needed. Because they are partially submerged, these platforms are very stable in rough seas. They are also strong and cost-effective[39].

Numerous companies and institutions are researching and developing semi-submersible floating platforms for offshore wind applications, and multiple of these platforms have been deployed for commercial use. Principle Power rolled out its 4th generation of WindFloat design and achieved an operational track record of exceeding 200,000 hours since its installation in 2011[40]. X1 Wind is a Spanish company specializing in floating wind technology. They have developed a unique floating platform design called PivotBuoy, and completed testing of this prototype in 2023 [41]. OCG-Wind platform, developed by Archer Wind is another example of the commercialisation of SSPs [42].

University of Maine designed a SSP, named DeepCwind platform, Figure 7., which was extensively researched and tested, with the help of multiple collaborators, intending to develop a robust SSP as a foundation for floating platforms[43]. This platform has exhibited great results during its testing and experimentation phase. Quality data from these experiments is publicly available for researchers to use this platform for individual research, as well as validation[44-47]. This platform has been used for this study.

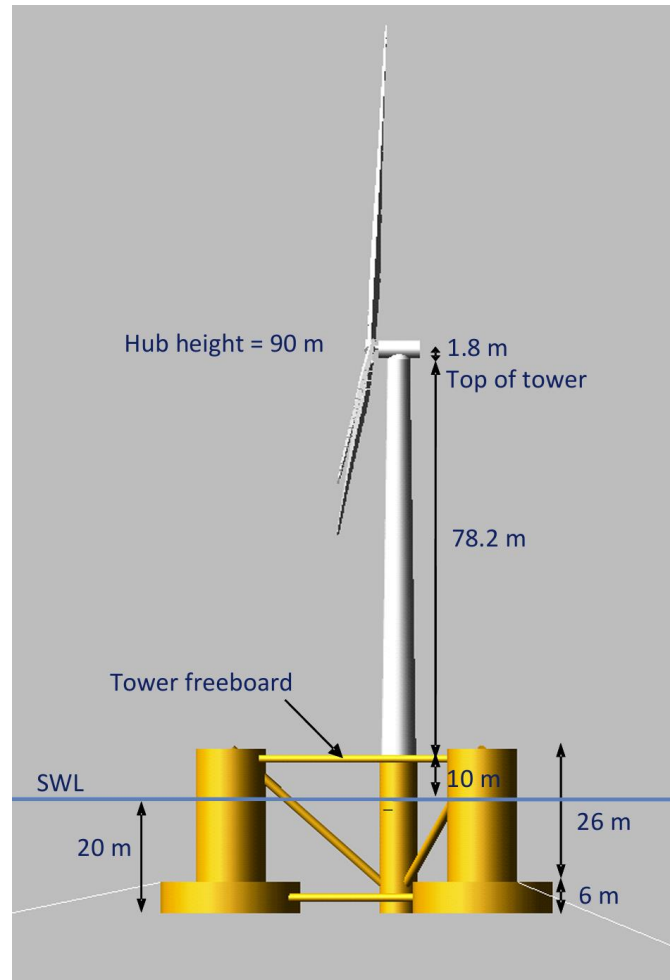


Figure 7. DeepCwind floating platform

2.2.3 WECs

WECs are widely classified based on several criteria, primarily focusing on their operational principles and the type of wave energy they harness. The classifications often overlap because WECs can be designed to fit multiple criteria. For example, a point absorber can be used both nearshore and offshore, and an oscillating water column can be classified by its operational principle and its location. The diversity in WEC designs and their adaptability to different environments and wave conditions make it challenging to fit them into a single, rigid classification system. Instead, the various classification methods provide a flexible

framework to understand and compare the different technologies based on specific aspects like location, operational principle, and energy conversion method [19, 48-50].

This study utilises the concept of PAWECs and they are classified as shown in Figure 8. These classified based on various criteria, including design geometry, deployment manner, and operating degrees of freedom (DoFs). They can be one-body or multi-body devices, with one-body PAWECs further divided into floating and submerged types. Floating one-body PAWECs, like the Seabased and CorPower devices [51, 52], interact with surface waves, while submerged one-body PAs, such as the AWS and CETO devices [53, 54], capture energy below the water surface. Multi-body PAs include self-reacting and self-contained types, with examples like the OPT PowerBuoy and Wavebob devices [55, 56]. PAWECs also vary in their power take-off (PTO) mechanisms, including hydraulic, mechanical, direct-drive, and novel systems like dielectric elastomers and triboelectric nanogenerators. Control strategies for PAWECs are essential for optimizing energy capture, adapting to varying wave conditions, and ensuring device survivability in extreme sea states.

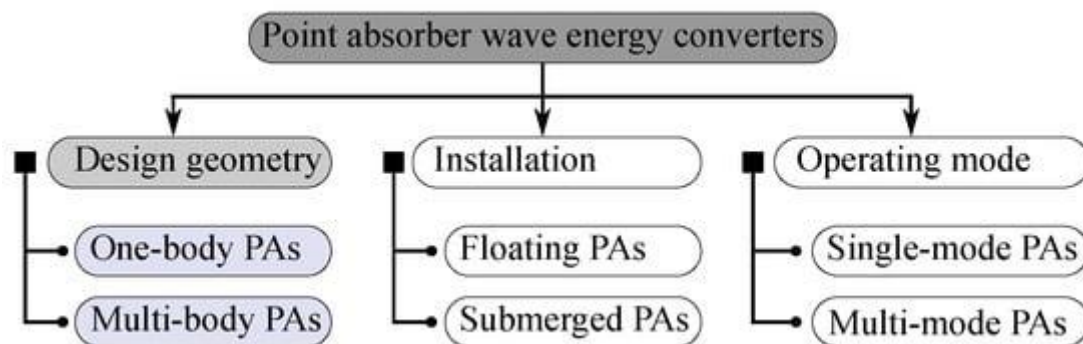


Figure 8. Classification of PAWECs[57]

This study focuses on the classification based on design geometry as it forms the basis for the design of the WEC. This study on axisymmetric point absorber [58], shows that shapes that protrude outward below the waterline generally perform better due to higher heave damping coefficients and according to [59], a concave shape results in the best dynamic responses and highest power production.

2.2.4 HWWFP

There are a number of concepts for WECs but the growth of this sector has been hindered, mainly due to the unfeasible economics but it is known that floating offshore wind is on the rise, and with the infrastructure that grows with it WECs can become feasible [12]. Apart from feasibility, there are studies that showcase other benefits of these novel systems. Like this study [60] concludes that WECs can compensate for wind power when wind speed is lower than rated wind speed. So, this concept increases the power production capacity by

6% without having any significant hinderance to its stability. A more relevant study which aligns with this study is presented in [61]. It employs a similar design concept of SSP with heaving WECs, and tests different WEC configurations. The study finds that larger WECs capture more energy, for specific sea states and the unfavourable effect of pitching moment is reduced after the addition of WECs. Out of the multiple WECs, the use percentage for oscillating body converters accounted for 58%, as compared to 34% for oscillating water columns and 8% overtopping WECs, this study finds [62]. It also talks about how research going on in this field can be categorised. These categories are (i) potential assessments of hybrid wind–wave explorations; (ii) hydrodynamic studies on substructures such as wave energy converters, wind turbines, and floating or bottom-fixed platforms; and (iii) the power preferences of their integrated systems.

Along with the research going on in this field, there are also so concept which have been tested out experimentally. The EU FP7 MARINA project tested 2 concepts for combined wind-wave systems [63]. This research [64] studied a Spar Torus Combination (STC) and concluded that There was a good agreement between the numerical and experimental results, confirming the accuracy of the numerical model. This study also concluded similarly and showed that there was no effect on the mooring lines, or the acceleration of the nacelle, or the bending moment at the tower's base [65]. The scope for research and development in this sector is immense. More experimental research and investment could famously provide a boost, and even reach commercial feasibility.

Based on this background, this thesis hopes to accomplish and validate some of the concepts numerically.

3. Methodology

The methodology section details the approach and tools used to conduct the research. This includes the selection of the reference site for simulation, design parameters of the floating platform and WECs, and system properties. A detailed description of the computer-aided design (CAD) of the platform, hydrodynamic modeling using Ansys AQWA, and time-domain simulations using WEC-Sim is provided. This section is critical for understanding how the study was conducted and the validation methods used to ensure accurate results.

3.1 Reference site

To ensure the successful deployment of a HWWFP, it's essential to have a thorough understanding of the wave energy resource and characteristics at the chosen site. This information helps assess the site's suitability for harnessing wave power, considering factors like wave height, period, direction, and environmental factors. Typically, data is

available from buoys placed near existing offshore rigs or data-collecting buoys. The other option is data offered by Copernicus Marine Service. It is a European Union (EU) program that provides free and open access to marine data and information. It is part of the Copernicus Earth Observation Programme, which aims to provide reliable information about the Earth's environment and climate. A lot of data from satellites, ground stations, aircraft, ships, and computer models are being used to provide information that helps people around the world. This information is available for free to anyone who wants to use it [66].



Figure 9. Site location

The reference site used for this study was offshore location in the Irish waters as seen in Figure 9. The location, 53.226°N and 11.843°W , is about a 100 kms off the coast of Ireland, and has depth of 200 m. This study has been conducted using E.U. Copernicus Marine Service Information [67]. GLOBAL_REANALYSIS_WAV_001_032 for the global wave reanalysis describing past sea states since years 1993. Sea surface wave significant height (H_s) and sea surface wave period at variance spectral density maximum, energy period (T_e), these are the two variables are analysed over a 4-year period to obtain a range of sea states for the study. A Joint Probability Distribution (JPD) has been produced for the two variables as seen in Figure 10., which indicates the probability of H_s and T_e for the selected location. The plot shows a clear concentration of probability in the lower left, indicating that waves with shorter periods and smaller heights are more likely to occur. The distribution has a tail extending towards the upper right corner, indicating that there is a possibility of

encountering waves with both high peak periods and significant wave heights, although these combinations are less likely. The dominant waves fall between peak period 6 and 13 s with significant wave height of 0.75 to 5 m. The average for H_s and T_e was 3.28 m and 11 s respectively.

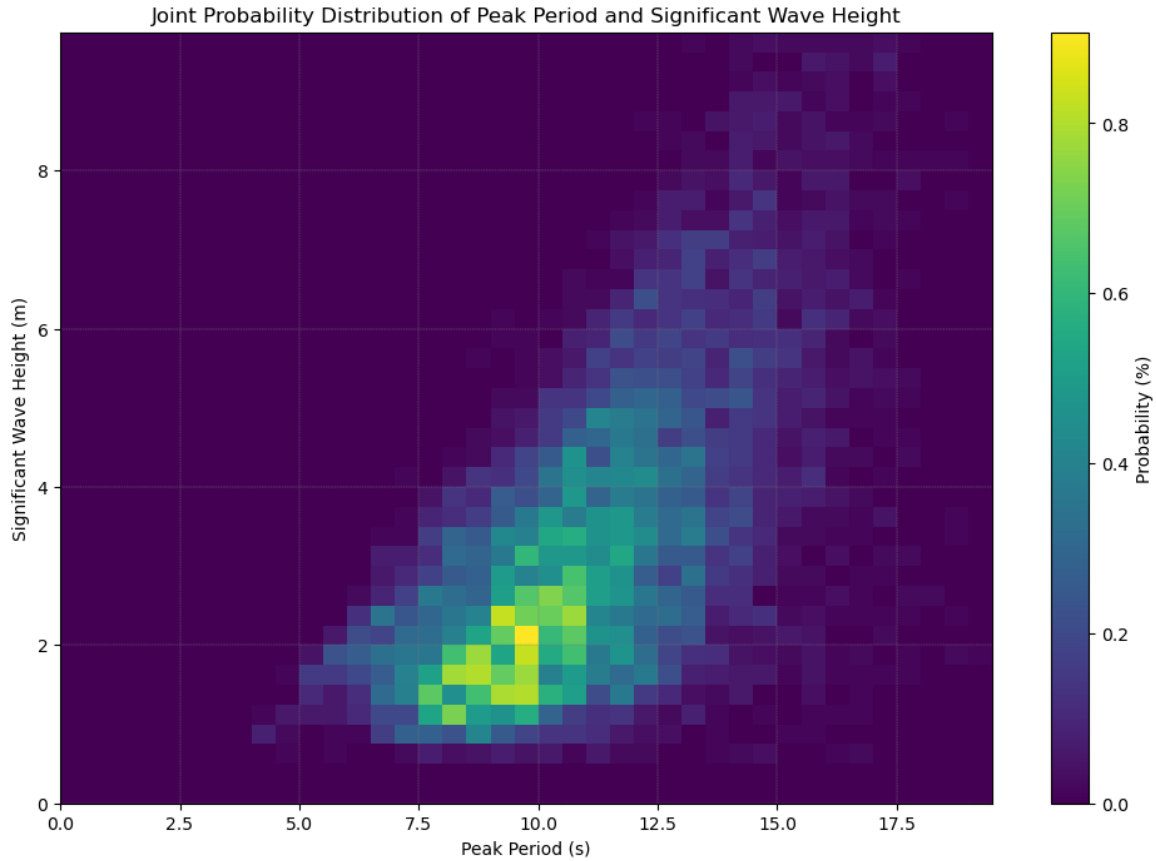


Figure 10. Joint probability distribution between Significant wave height and Peak period.

The range for the diameter of the buoy is determined based on the maximum possible energy absorption from the incident waves and the wave characteristics at the installation site. The maximum capture width ratio, a non-dimensional term, is recommended by this given equation in [23]:

$$C_{wr} = \frac{L_{max}}{D} \geq 3 \quad (10)$$

Where, D is diameter of WEC, L_{max} is the maximum capture width of WEC. The maximum energy that may be absorbed by a heaving axis symmetric body equals the wave energy transported by the incident wave front of width equal to the wavelength divided by 2π . So, L_{max} can be defined as:

$$L_{max} = \frac{\lambda}{2\pi}$$

(11)

the maximum wave power P_{max} , absorbed by a heaving axisymmetric body can be given as follows:

$$P_{max} = JL_{max}$$

Where J is energy flux. For linear deep waters:

$$J = \frac{\rho g^2 T H^2}{32\pi} \quad (12)$$

$$\lambda = \frac{gT^2}{2\pi} \quad (13)$$

From equation (9), (10), (11) and (12) and the period range determined for the reference site, the upper bound limit for 13 s is $D \leq 14$ m. The lower bound limit is given as $D \geq 4$ m.

3.2 Design parameters

3.2.1 Orientation and coordinate system

It is important to note that all the structures designed need to follow the right orientation as followed by ANSYS coordinate system, where the system is designed with Z axis as vertical and -Z axis is gravity. +X axis is the direction of wave propagation. The origin of the Z axis is at the Surface Water Level (SWL). The motions and orientation are explained in Figure 11. These settings remain constant for all designs and simulations.

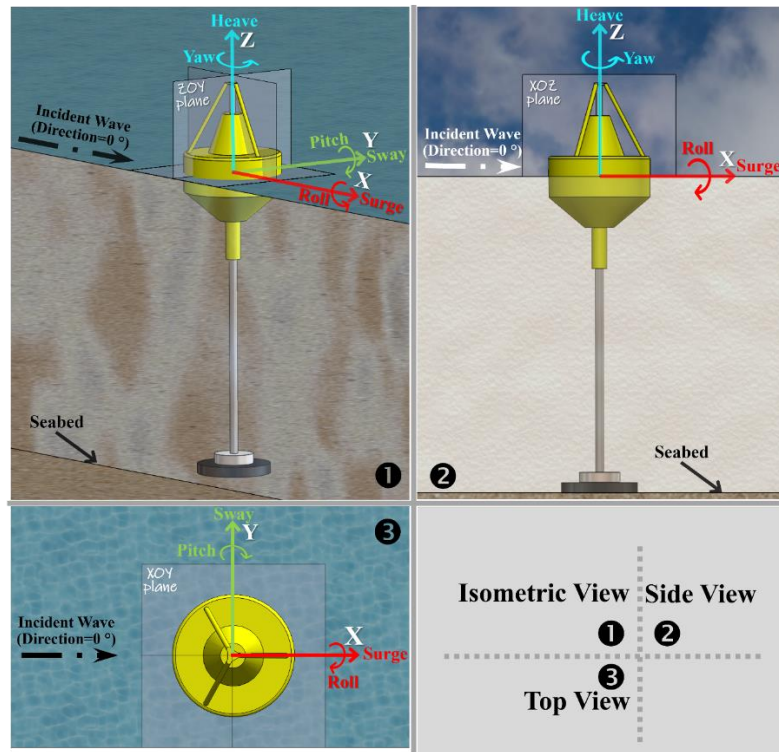


Figure 11. Coordinate system

3.2.2 SSP

As mentioned in section 2.2.2, DeepCwind platform has been chosen as the floating platform on which the WECs will be mounted. The structures are defined in Figure 12. The 3D model of the platform was done using SolidWorks and the parameters are mentioned in Table 1.

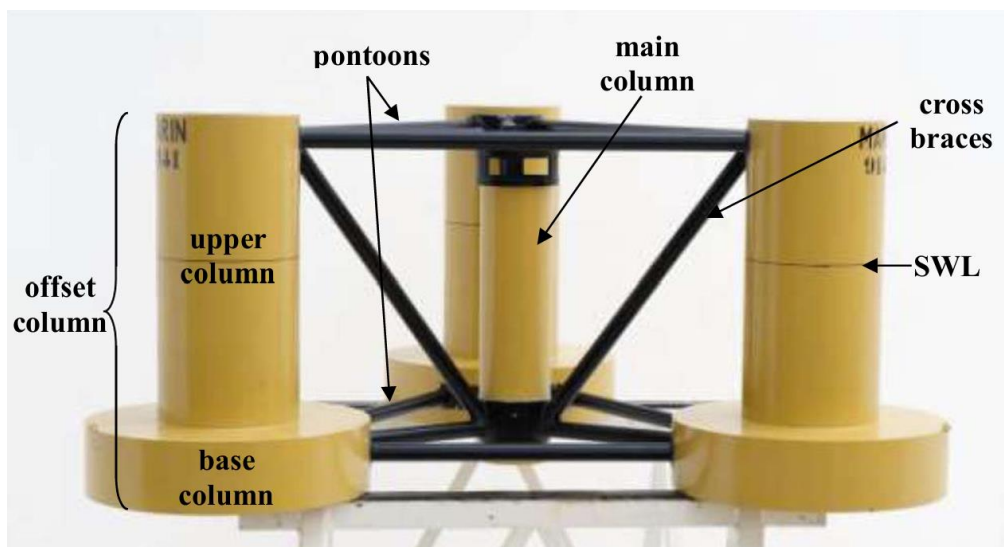


Figure 12. Structures of SSP

Parameter	Value
Depth of platform base below SWL (total draft)	20 m
Elevation of main column (tower base) above SWL	10 m
Elevation of offset columns above SWL	12 m
Spacing between offset columns	50 m
Length of upper columns	26 m
Length of base columns	6 m
Depth to top of base columns below SWL	14 m
Diameter of main column	6.5 m
Diameter of offset (upper) columns	12 m
Diameter of base columns	24 m
Diameter of pontoons and cross braces	1.6 m

Table 1. Design parameters for SSP

3.2.3 WECs

The external geometry of the WEC is similar to a truncated cone. This was designed based of the points discussed in section 2.2.3. Table 2. Shows the design parameters for the WEC. The WEC is hollow, and the linear PTO is placed within the WEC. The PTO system is positioned towards the bottom of the device and the lowers the CM

Parameter	Value
Depth below SWL (draft)	6 m
Elevation above SWL	6 m
Diameter (maximum)	12 m
Diameter (minimum)	3

Table 2. Design parameters for WEC

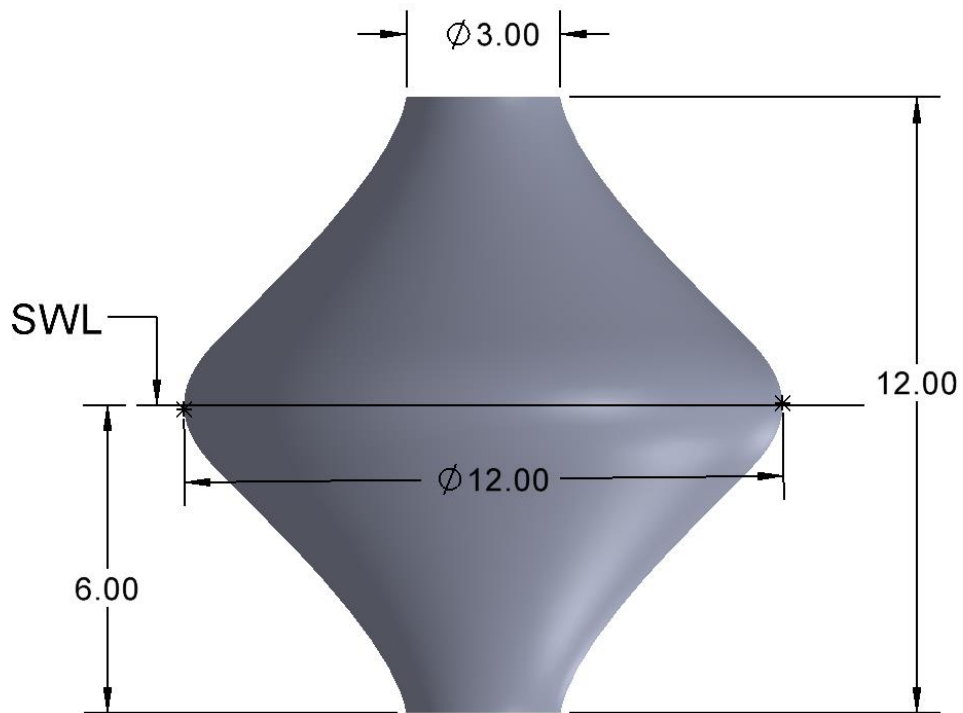


Figure 13. WEC dimensions

3.2.4 HWWFP

Two vertical pontoons are added between the upper and the lower pontoons, which will guide the heaving motion of the WECs. Figure 14. shows the layout of WECs. The distance

Parameter	Value
Distance from centre of upper column	16.5 m
Distance between centres of WECs	17 m
Gap between WECs	4 m

Table 3. Design parameters for HWWFP

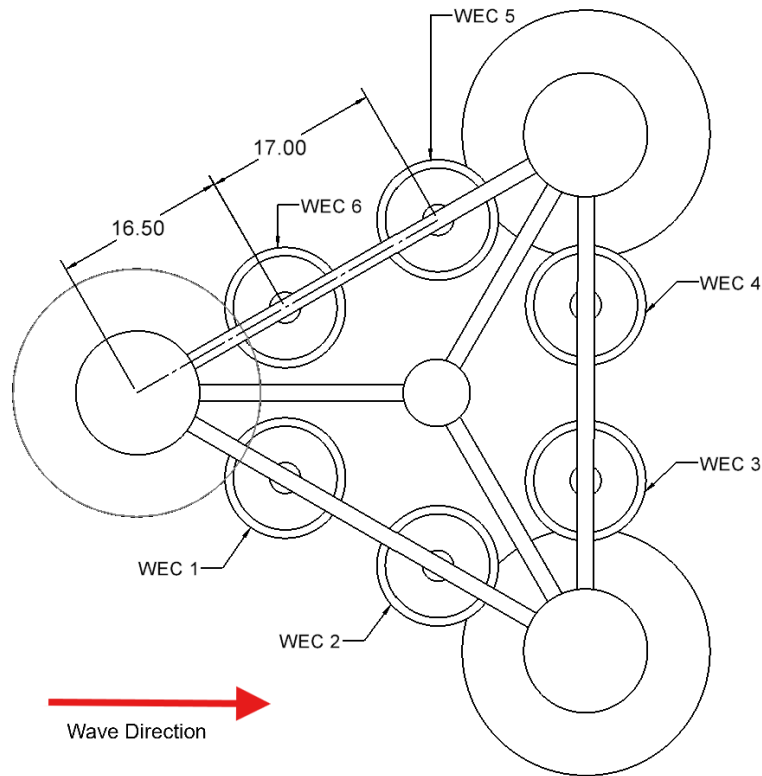


Figure 14. HWWFP layout

3.3 System properties

As mentioned in section 2.1.4, BEM is used in AQWA and a meshing is performed for the same. The mesh statistics are mentioned in table 4. BEM does not mesh solid bodies, so all solid bodies from SD are converted to surface bodies. The maximum element size for meshing has a limit in AQWA, which also limits the maximum allowable frequency to be considered in simulations. Although, the simulation is run for the frequencies for the data obtained at the reference site, and the upper limit of the range is within the maximum allowable frequency. A separate “Natural modes” solution is run to validate the natural frequencies of the SSP. Further, to perform HD in AQWA, the simulation parameters needed to be set up. A simulation was run for the SSP and HWWFP to obtain, and compare, coefficients like added mass, radiation damping and wave excitation forces. The parameters are mentioned in table 5. It should be noted that for SSP simulation, the total mass properties, which include the 5 MW wind turbine, were used so as to validate the study results with the actual results.

Properties	Value
Total mass of SSP	1.3958E+7 kg
Displacement SSP	1.3917E+4 m ³
SSP CM location below SWL	8.07 m
SSP roll inertia about CM	1.3947E+10 kg-m ²

SSP pitch inertia about CM	1.5552E+10 kg-m ²
SSP yaw inertia about CM	1.3692E+10 kg-m ²
Mass of each WEC	17700 kg
WEC CM location below SWL	3 m
WEC roll inertia about CM	312924.78 kg-m ²
WEC pitch inertia about CM	314084.35 kg-m ²
WEC yaw inertia about CM	316647.54 kg-m ²

Table 4. Properties of SSP and WEC

ANSYS AQWA has a limit on the total number of elements for HD, which is 40,000. Given the dimensions of the structure, the generated mesh is coarse, and this directly affects the accuracy of the results. Table 5. Shows the mesh statistics for SSP and HWWFP. The element size had to be reduced in HWWFP after adding the 6 WECs. Figure 15. displays the meshed HWWFP.

Parameter	Value
SSP mesh element size	0.55 m
SSP mesh elements	35761
HWWFP mesh element size	0.58 m
HWWFP mesh elements	39375

Table 5. Mesh details

All the parts were assigned their own local coordinate system at the centre of mass within the meshing component because local coordinate systems help in accurately defining the geometry and orientation of parts, especially if they are not aligned with the global coordinate system. Applying boundary conditions, loads, and constraints can be more straightforward when using a local coordinate system. This is particularly useful for complex structures or assemblies, such as this study.

Most of the values for the environment of the simulation are default, values need to be changed before solving the simulation. Some values are defined, as mentioned in table 6.

Parameter	Value
Water depth	200 m
Water density	1026 kg/m ³
Acceleration due to gravity	9.81 m/s ²

Table 6. Simulation parameters for HD

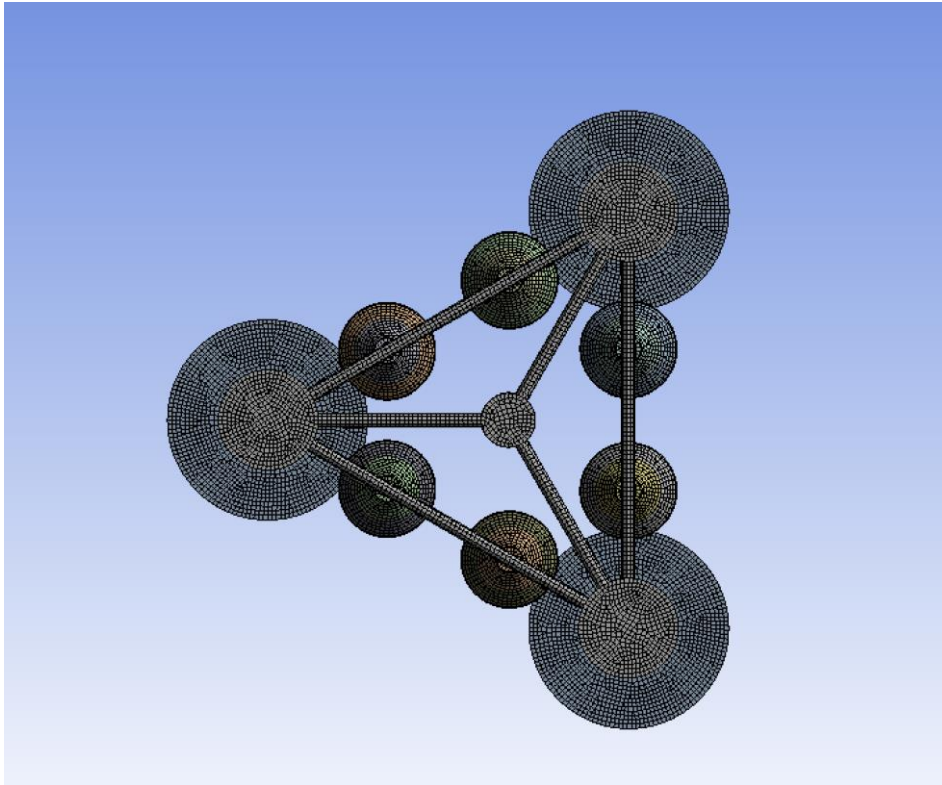


Figure 15. Meshed HWWFP

At this step, the model is ready to be simulated in HD AQWA. All of the above sections can be summarized as pre-processing steps in a workflow for hydrodynamic analysis.

3.4 Power generation

In this study, the focus is on analysing the wave energy conversion aspect of a wind-wave hybrid platform, specifically excluding the wind generation component. The simulation process involves using WEC-Sim to evaluate the performance of the WECs under various sea conditions.

These sea states are representative of the conditions at a specific reference site, which has been analysed to provide realistic wave height and period data. The simulations cover a comprehensive range of sea states to ensure that the performance of the WEC is thoroughly evaluated under different wave conditions. WEC-Sim performs time-domain analysis, solving the equation (9) for the WEC system in six DOFs. The hydrodynamic coefficients, such as added mass and radiation damping, are derived from BEM based potential flow solvers. These coefficients are essential for accurately modelling the interaction between the WEC and the waves.

3.4.1 BEMIO

BEMIO (Boundary Element Method Input/Output) in WEC-Sim is essential for processing hydrodynamic data from BEM solvers like AQWA. It converts this data into a format usable by WEC-Sim, which is .h5, calculates impulse response functions (IRFs), and performs state space realization for efficient time-domain simulations. BEMIO ensures accurate and reliable input data, enhances computational efficiency, and supports multiple BEM solvers, making it a crucial component for accurate and efficient modelling of wave energy converters. WEC-Sim scales the hydrodynamic coefficients according to these equations:

$$|\overline{F_{ext}(\omega)}| = \frac{|F_{ext}(\omega)|}{\rho g}$$

$$\overline{A(\omega)} = \frac{A(\omega)}{\rho}$$

$$\overline{B(\omega)} = \frac{B(\omega)}{\rho \omega}$$

$$\overline{K_{hs}} = \frac{K_{hs}}{\rho g}$$

Where K_{hs} is linear hydrostatic restoring coefficient.

The MATLAB code to obtain the BEMIO file can be found in Appendix A.

3.4.2 Simulink model

The Simulink modelling for the hybrid wind-wave platform involved several key components to accurately simulate the system's dynamics. The model included an "Active Method: Input File" block, which specified the input file containing the simulation parameters, such as wave characteristics and PTO settings. Constraint blocks were used to represent the constraints applied to the system, such as mooring lines or fixed points, which limited the movement of the WEC components.

Body blocks, labelled from body (1) to body (7), represented different parts of the platform, including the floating structure and WEC components. Each body block included hydrodynamic properties and mass characteristics essential for simulating the physical behaviour of the system. PTO blocks simulated the energy conversion mechanisms, converting mechanical energy from the WEC into electrical energy.

The connections between these blocks represented the physical and data interactions within the system, ensuring that the dynamics of the platform and its components were accurately modelled. The SSP was connected to the seabed through a 6 DOF constraint

block and the WECs were connected with a translational PTO since there is only a heaving motion DOF for the WEC. This setup allowed for a comprehensive simulation of the wave energy conversion process. The Simulink model can be found in Appendix A.

3.4.3 PTO

A Linear PTO is employed in this study, which is available in wec-Sim. In the context of a heaving point absorber WEC, the device moves vertically with the rise and fall of ocean waves. A linear PTO directly captures this vertical (or heaving) motion, as opposed to rotational PTO systems that convert wave motion into rotational energy. This linear PTO system is simple spring-damper mechanism. The spring component in the PTO stores energy from the wave-induced motion, much like a conventional spring stores potential energy when compressed or stretched. In the case of a wave energy converter (WEC), the spring absorbs and stores energy during the heaving motion of the device. When the WEC moves due to a wave, the spring compresses or stretches, and then releases that energy as the wave subsides. The damper, on the other hand, dissipates energy, typically converting it into a useful form, such as electrical energy. The damper resists the relative motion between the WEC and the PTO, and this resistance helps to extract energy from the system. The force exerted by a Power Take-Off (PTO) system modelled as a spring-damper is calculated based on the combined contributions of the spring and damper components. The total PTO force, F_{pto} , is the sum of the forces from the spring and damper, which depend on the displacement and velocity of the system, respectively. The general equation is:

$$F_{pto} = -K_{pto}X - B_{pto}\dot{X}$$

Where K_{pto} is spring stiffness, B_{pto} is damping coefficient, X is displacement of WEC from equilibrium position and \dot{X} is the rate of displacement.

In many WEC systems, the K_{pto} is often considered as zero in the PTO system, especially for linear PTO designs. It is done to ensure the WEC moves freely with the waves, maximizes energy absorption through pure damping, simplifies the system's dynamics, and leverages the natural buoyancy of the device as a restoring force. By focusing only on damping, the PTO can efficiently convert the wave-induced motion into usable energy without interference from spring-like forces [68].

The energy extracted from the waves is proportional to the relative motion, and the damping coefficient determines the balance between excessive resistance and optimal energy absorption. Equation (14) represents the analytical approach to find the optimal damping coefficient for a single heaving body [61].

$$B_{pto} = \sqrt{\frac{((m + A_{3,3})\omega^2 - (K_{pto} + F_B))^2}{\omega^2} + B_{3,3}^2}$$

(14)

Figure 16. shows the plot obtained using the above equation. The respective values of optimal PTO damping coefficients are incorporated while defining the sea states mentioned in Table 8

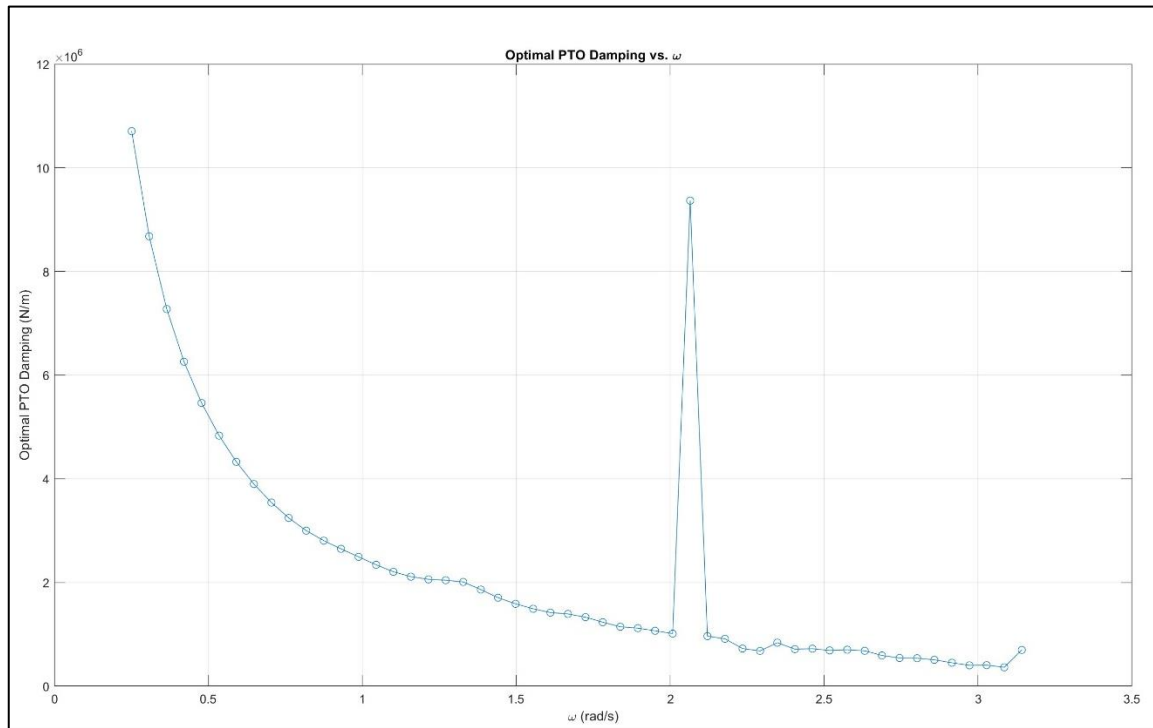


Figure 16. Optimal PTO damping coefficient for WECs

3.4.4 Inputs

Wec-SIM gives a lot of freedom with the simulation inputs. All the input parameters as defined in a single input file. The details of this MATLAB script is available in Appendix A.

The `wecSimInputFile.m` is essential for setting up the simulation environment in WEC-Sim. It ensures that all necessary parameters and properties are correctly defined, enabling accurate and efficient simulations. By organizing the simulation setup in a structured manner, this file facilitates the integration of various components, such as wave conditions, body dynamics, and PTO systems, into a cohesive model.

The key parameters defined for this study are given in table 7.

Parameter	Value
Fixed time step	0.04 s
End time	180 s

Ramp time	150 s
Wave class	Irregular
Wave spectra	'JS'
PTO stiffness	0

Table 7. Input parameters for Wec-SIM

A fixed time step was preferred due to the simplicity and consistency. Since the reference site for the model simulation is in the deep seas, an irregular wave class was chosen. Irregular waves better represent the complex and random nature of real ocean waves compared to regular waves, which are idealized and less representative of actual sea conditions. As for the wave spectra, JONSWAP (JS – Joint North Sea Wave Project) was selected. JS is specifically designed to model the energy distribution of waves in deep sea states. Using the JS spectrum allows for a more accurate representation of the wave energy environment, leading to better predictions of the WEC's performance. The JS spectrum is widely accepted and used in the marine and offshore industries for wave modelling. Its use in this simulation aligns with industry practices, ensuring that your results are credible and comparable to other studies [69].

Once the WEC model is constructed, the SimMechanics 6DOF multi-body solver performed the simulation by summing forces from time domain modules at each time step and advancing the simulation in time using a 4th-order Runge Kutta integration scheme [70].

To evaluate the power performance of the WEC system, three representative sea states were selected based on data from the reference site. Each sea state is characterized by its significant wave height and peak wave period. These parameters correspond to the dominant conditions at the site and allow for the performance analysis of the WECs under realistic operating scenarios. The range of the SS is within the range of the reference site and can be referred to in Table 8.

Sea State	Wave period	Wave height	B_pto
SS1	7.5 s	1.7 m	2.81E+06 (N/m)
SS2	10 s	2.2 m	3.90E+06 (N/m)
SS3	11.2 s	3.5 m	4.83E+06 (N/m)

Table 8. Sea states definition

4. Results and discussion

This section presents the outcomes of the simulations and analyses. It discusses the hydrodynamic performance of the hybrid floating platform, comparing the Response Amplitude Operator (RAO) results for different motions (surge, heave, and pitch). The discussion highlights key findings, such as the reduction of pitch motion due to the integration of WECs and the overall improvement in platform stability. The power performance analysis is also covered, detailing how different wave conditions and damping values impact energy production.

4.1 Hydrodynamic diffraction results

This section displays, and discusses the results obtained from HD AQWA. Comparative plots for SSP and HWWFP are generated. Analysing the frequency response for surge, heave, and pitch is more common than for sway, roll, and yaw due to the dominant nature and operational significance of these motions. Surge, heave, and pitch typically have more pronounced effects on the stability and performance of floating structures, directly impacting vertical and longitudinal stability, which are critical for marine operations. These motions also experience significant restoring forces due to buoyancy and gravity, making them essential for stability and resonance analysis. Additionally, heave and pitch affect vertical displacement and angular tilt, crucial for operations like energy extraction in wave energy converters and stability in floating wind turbines, while surge impacts forward and backward movement, important for mooring and station-keeping. Therefore, focusing on these motions helps in designing structures that can withstand wave-induced forces, maintain operational efficiency, and ensure safety and comfort for personnel on board.

All the results are plotted for the range of 4 to 17 s (0.37 to 1.571 rad/s), which covers the dominant range for the reference site of 6 to 13 s. Additionally, the data is analysed for the 0° wave direction, which is the wave heading towards positive X.

4.1.1 Validation for SSP

The model developed for SSP is simulated in HD AQWA to obtain the natural modes between the range of 0.01 Hz to 0.1 Hz. The results showed 3 peaks within this range, as mentioned in table 7 and figure 16. The model is validated with the experimental values from [15], for 3 degrees of freedom (DOF) heave, roll and pitch, before adding the WECs to the platform.

DOF	Experiment (s)	Study (s)
Heave	17.5	17.24

Roll	32.8	32.7
Pitch	32.5	33.8

Table 9. Comparison of AQWA with experimental results of 3 DOF motion natural periods

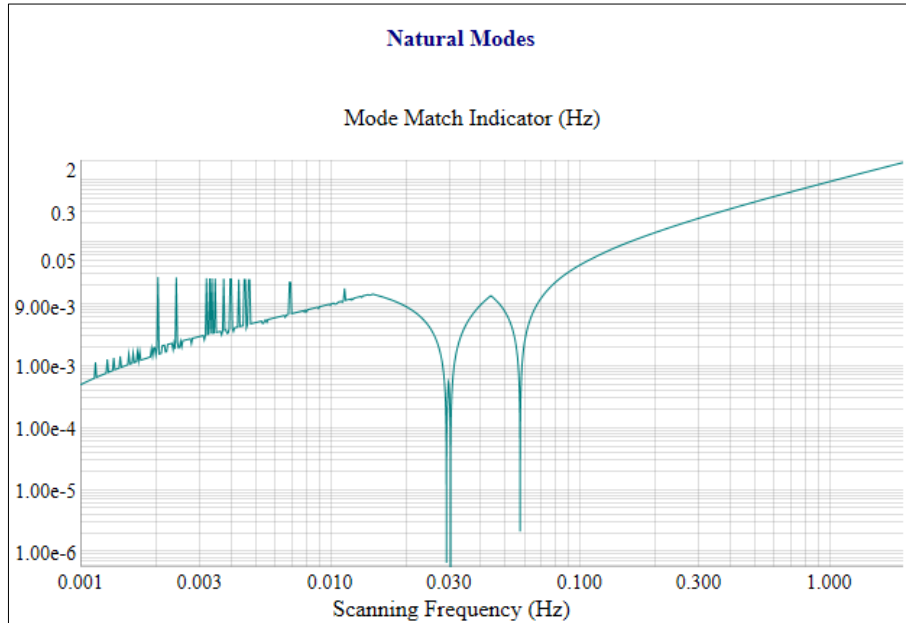


Figure 17. Natural modes for SSP

4.1.2 RAO

The Response Amplitude Operator (RAO) is a crucial measure in marine and offshore engineering that describes how a floating structure responds to wave excitation at different frequencies [16]. It quantifies the relationship between the wave input and the resulting motion of the structure, helping predict the motion responses such as heave, pitch, and surge under various wave conditions. RAOs are essential for designing and analysing the stability and performance of floating structures, ensuring safety and operational efficiency. Mathematically, RAOs are represented as the ratio of the amplitude of the structure's response to the amplitude of the wave excitation at a specific frequency.

$$\text{RAO}(\omega) = \frac{X(\omega)}{A(\omega)}$$

Where $X(\omega)$ is the amplitude of the response of the structure at ω and $A(\omega)$ is the amplitude of the incident wave.

For surge motion, in figure 17, it is observed that both the systems follow a similar trend of decrease in surge amplitude as the frequency increases up to around 0.6 rad/s for SSP and slightly higher for HFFWP. As frequency increases, both platforms show a decrease in

surge, but the SSP platform exhibits a more pronounced dip around 0.9 rad/s, suggesting a resonance frequency where the platform's motion is minimized. The HFFWP platform shows a steadier decrease in surge and a less pronounced dip, indicating that the presence of WECs helps in dampening the motion more effectively across a range of frequencies. The steadier response of the HFFWP platform suggests improved stability with the addition of WECs, as it experiences less variation in surge across different frequencies.

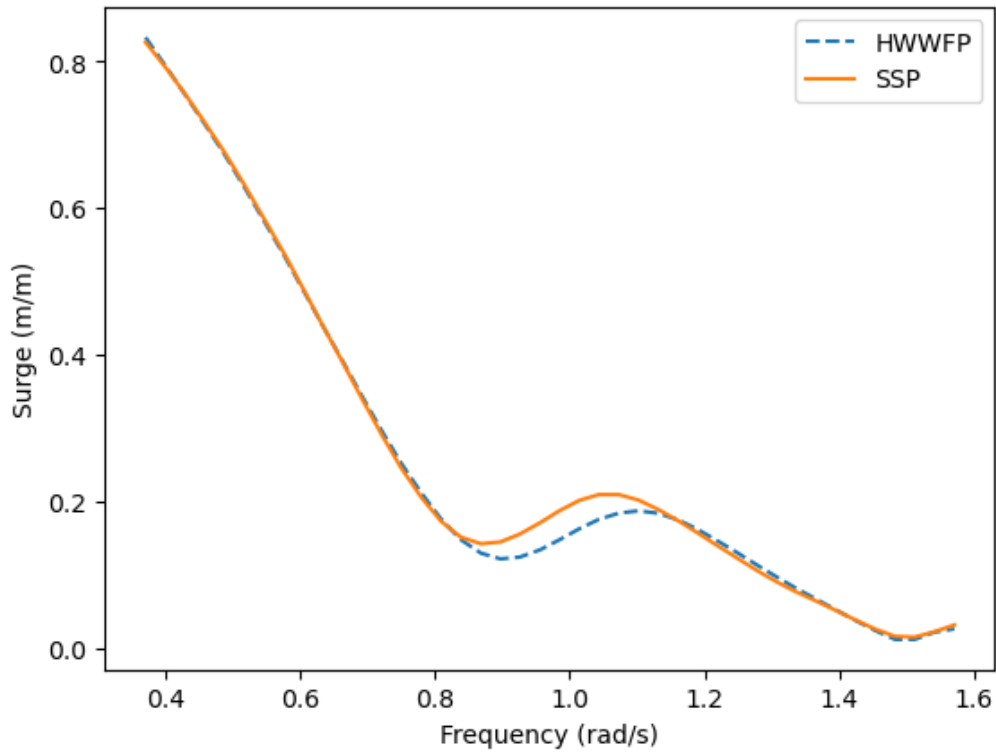


Figure 18. Surge RAO for SSP and HFFWP

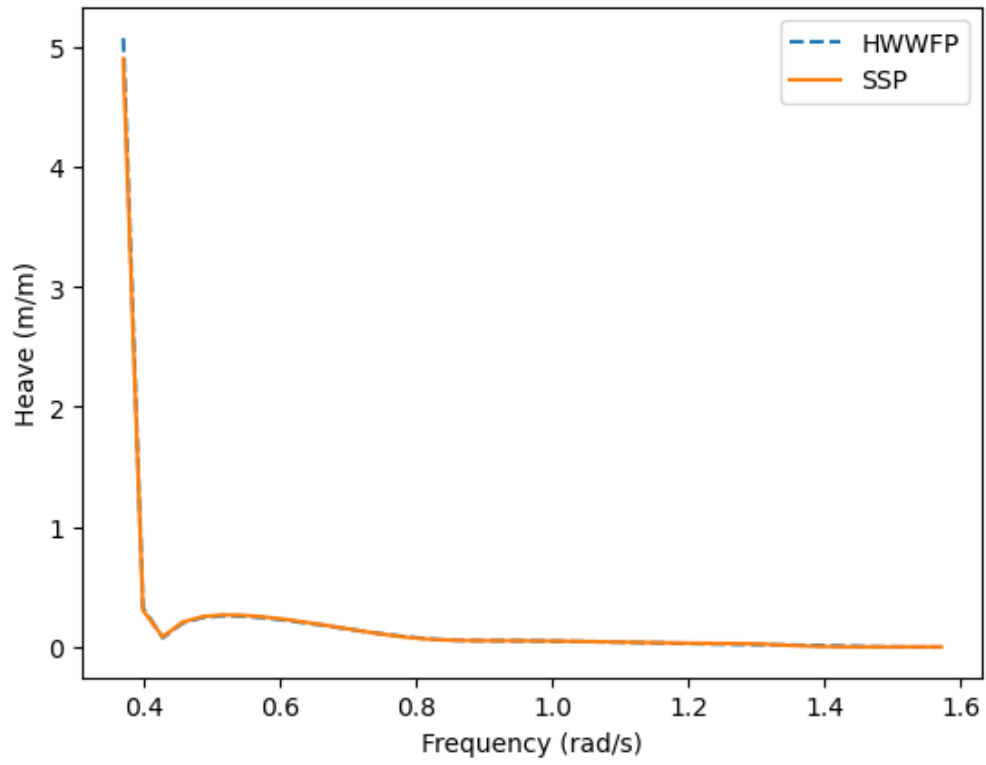


Figure 19. Heave RAO for SSP and HWWFP

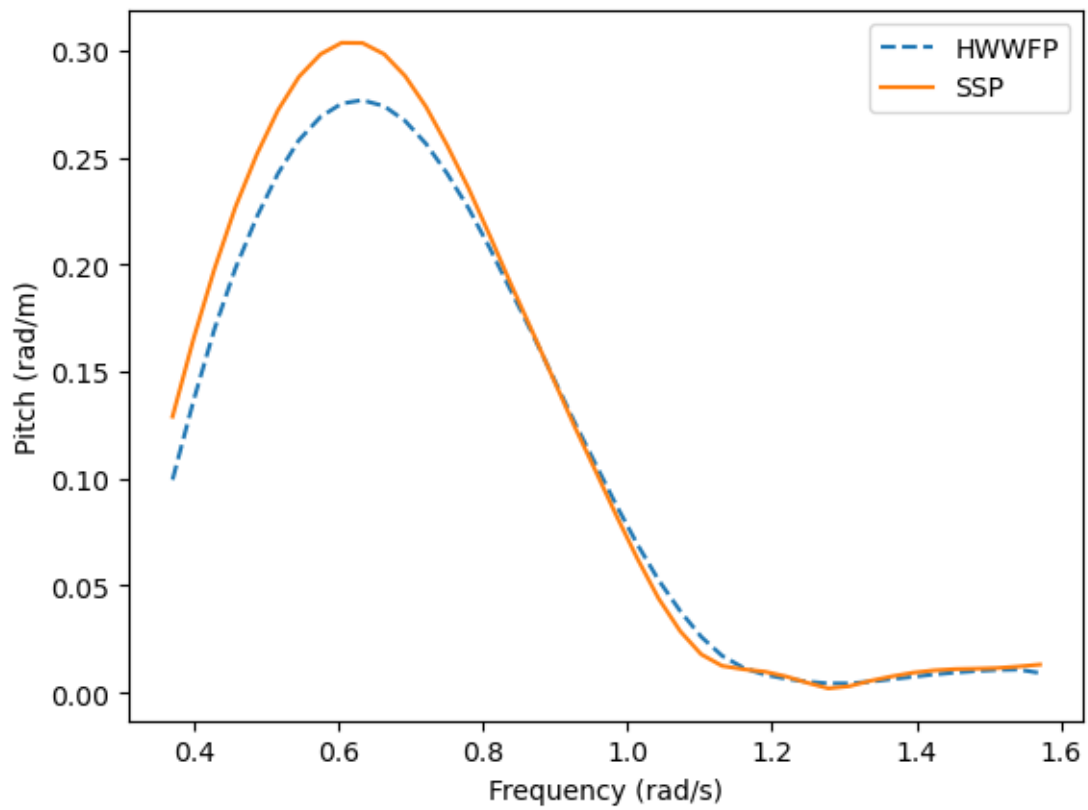


Figure 20. Pitch RAO for SSP and HWWFP

Both platforms exhibit nearly identical heave responses across the entire frequency range, indicating that the presence of WECs does not significantly affect the vertical motion of the platform, as seen in figure 18. Both curves start at a high heave value at the lowest frequency and sharply decrease as the frequency increases, flattening out at higher frequencies. This suggests that the platforms' heave motion is more pronounced at lower frequencies and stabilizes at higher frequencies. Also, the heave motion starts to peak at an even lower frequency, because it is close to its natural frequency for heave, as given in table 7, resulting in the steep decline we see in the plot. Due to this natural frequency, the RAO for heave has the highest value among the 3 motions.

The pitch response, in figure 19., exhibits a desirable result as the curve for HWWFP remains within the curve of the SSP, which shows that the WECs dampen the pitch response for the platform. Surge, heave and pitch motion reduce significantly with increasing frequency, and this is consistent with the other studies [61].

4.1.3 Hydrodynamic coefficients and forces

4.1.3.1 Radiation damping

Radiation damping refers to the energy dissipation that occurs when a structure or object moving in a fluid radiates energy away in the form of waves. It represents the loss of energy from the system due to the generation of outgoing waves and it most certainly affects the overall dynamics and stability of the structure.

Figure 20. shows the radiation damping for the surge component. At lower frequencies, both the systems have almost the same trend but at the higher frequencies, the values peak again for HWWFP. As for the radiation damping in heave, in figure 21., the curves are similar with some offsets at lower and higher peaks. The HWWFP radiation damping almost consistently remains higher than SSP, as shown in figure 22., the pitch damping component is slightly lower at the at smaller frequencies but they too follow the same trend.

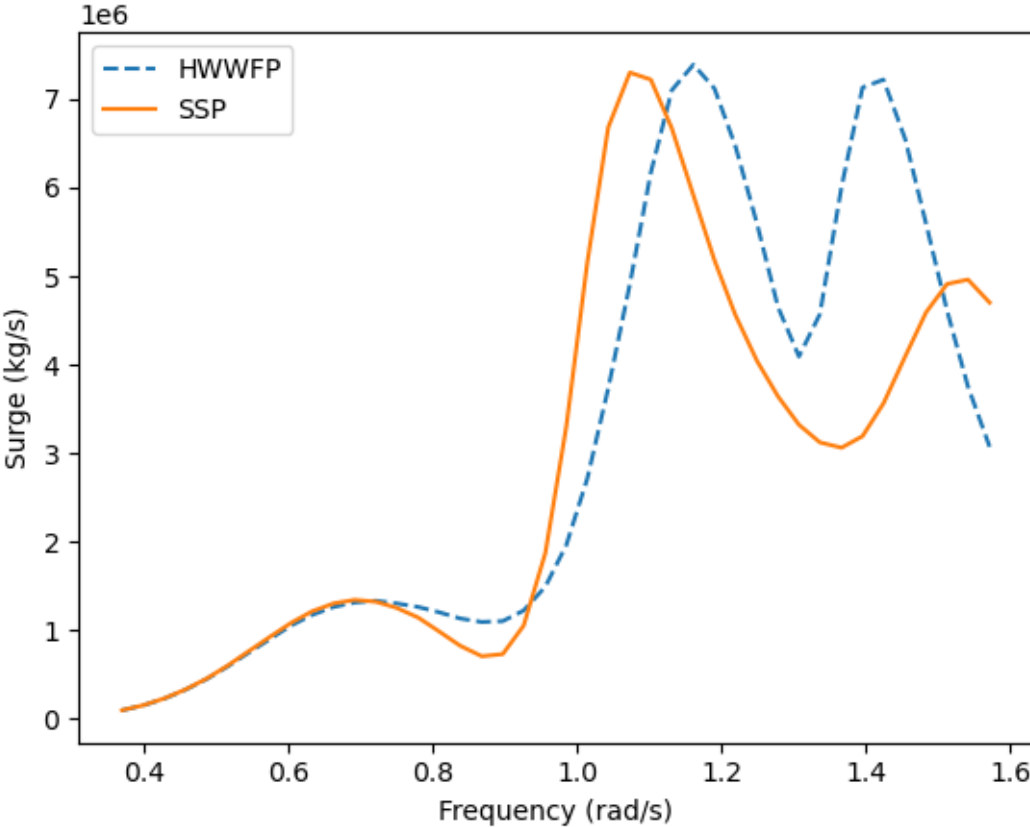


Figure 21. Surge component of radiation damping for SSP and HWWFP

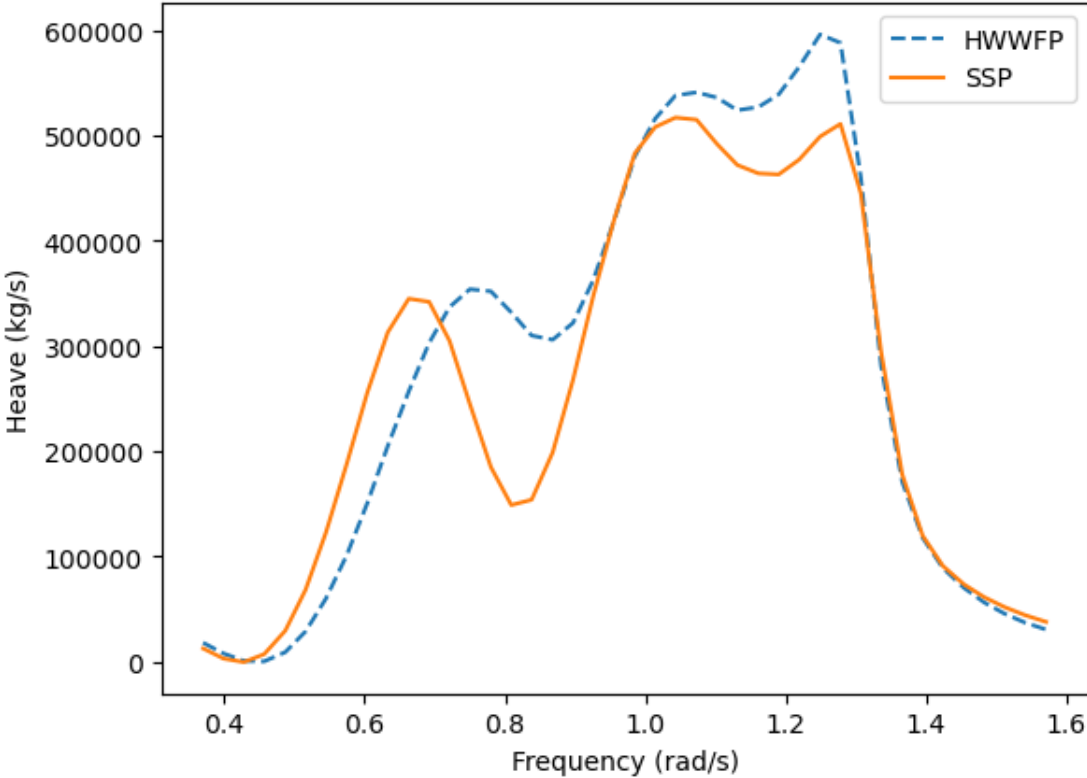


Figure 22. Heave component of radiation damping for SSP and HWWFP



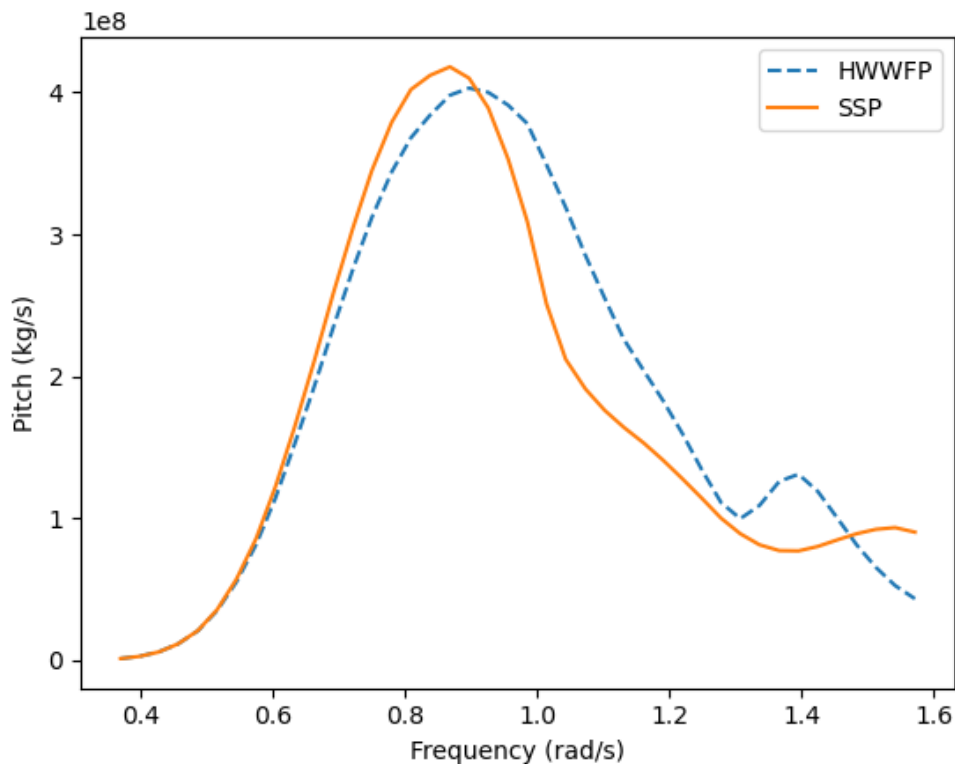


Figure 23. Pitch component of radiation damping for SSP and HWWFP

4.1.3.2 Hydrodynamic diffraction

Diffraction forces are hydrodynamic forces that arise when waves encounter a structure and are scattered or diffracted around it. When waves hit a structure, they are partially reflected, transmitted, and diffracted. The diffracted waves create additional forces on the structure.

Figures 23, 24 and 25 show the diffraction forces in the surge, heave and pitch components for SSP and HWWFP. The observation made from figures 23 and 24 is that at higher frequencies, these forces are higher for HWWFP than for SSP. This is primarily because higher frequency waves carry more energy, and the HWWFP system, with its Wave Energy Converters (WECs), presents a larger surface area for wave interaction. This increased interaction surface amplifies the diffraction effects, resulting in higher forces. Although the overall diffraction forces reduce across the two motions, the forces remain higher for the HWWFP system at these frequencies. As for the pitching component, the diffraction force is slightly lower for higher frequencies. The variation could be because the column of SSP is the first face to interact with the incoming wave at 0° . This suggests that while the WECs effectively interact with the waves, the system must be designed to handle these increased forces to ensure stability and efficiency. The WECs must be tuned optimally to absorb this energy at higher frequencies.

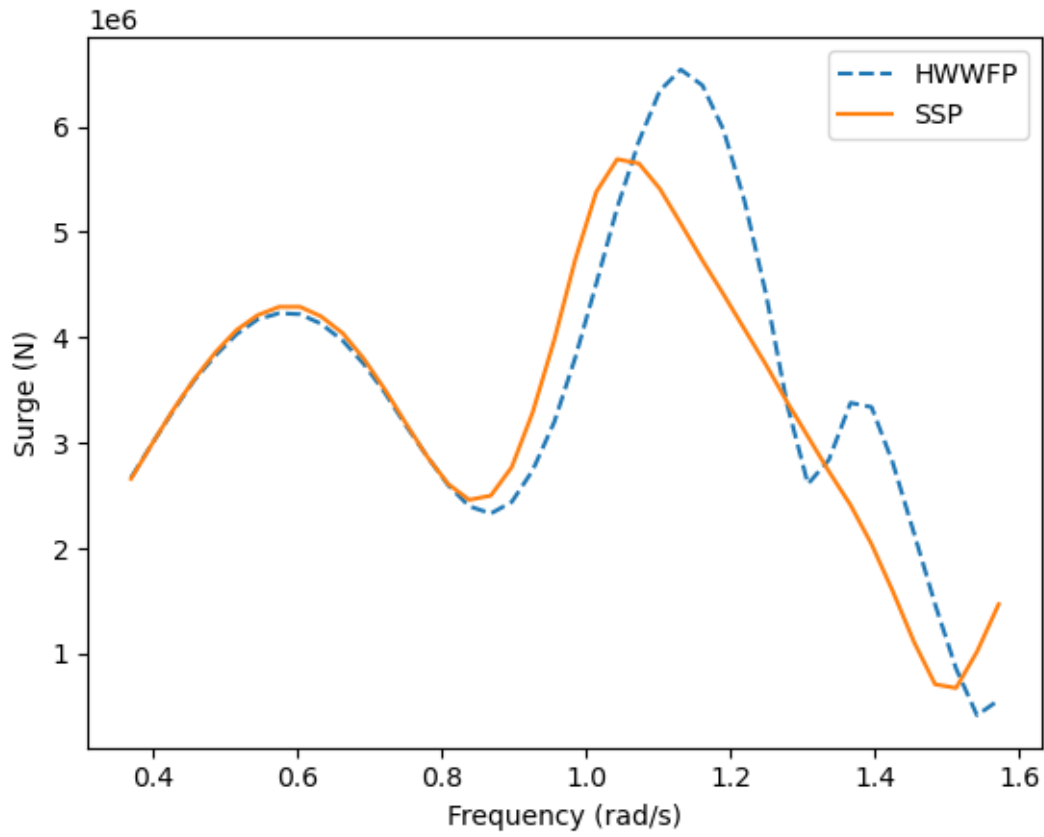


Figure 24. Surge component of hydrodynamic diffraction forces for HWWFP and SSP

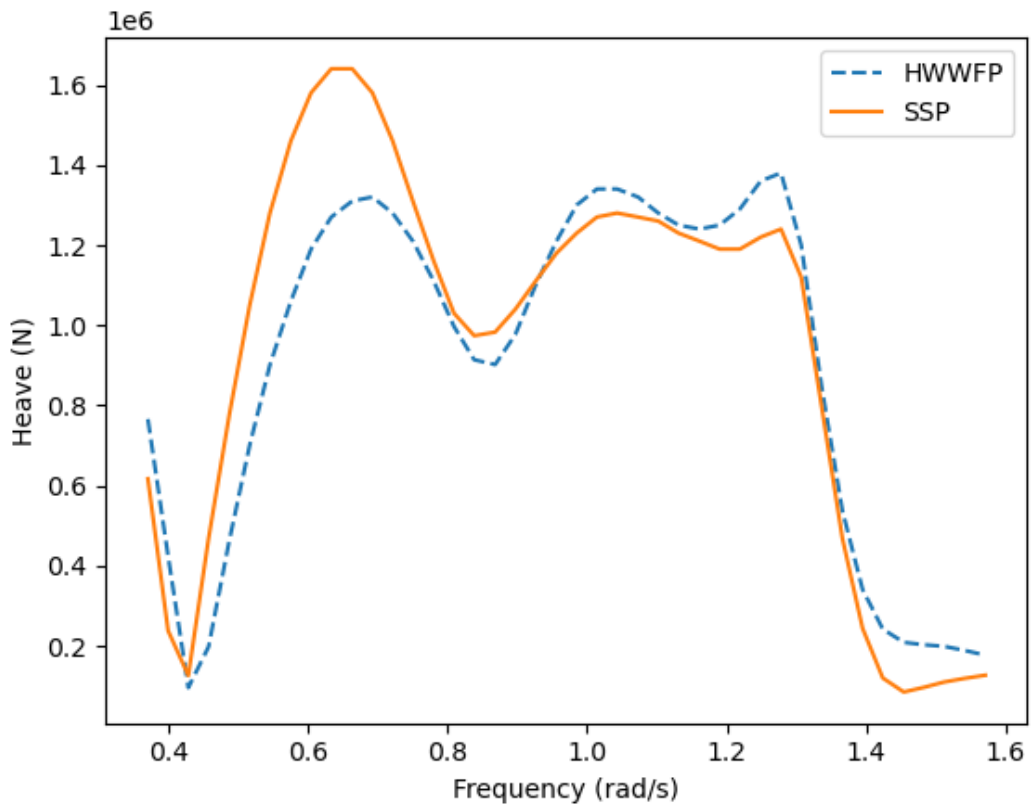


Figure 25. Heave component of hydrodynamic diffraction forces for HWWFP and SSP

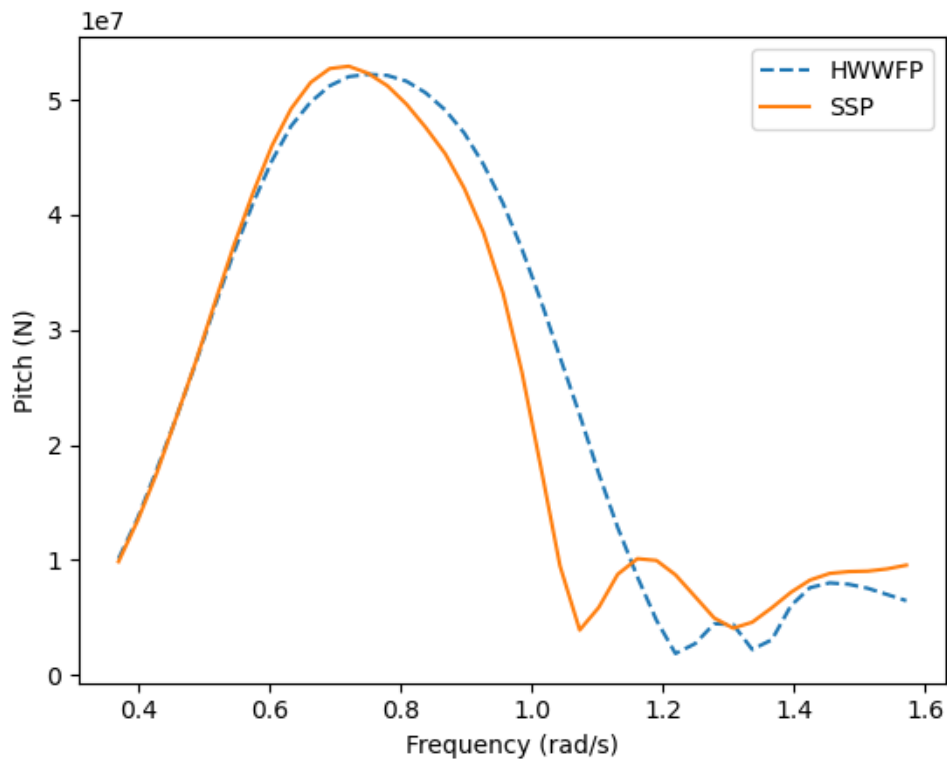


Figure 26. Pitch component of hydrodynamic diffraction forces for HWWFP and SSP

4.2 Time domain analysis

Given that SS3 has the highest wave period and significant wave height among the selected conditions, it is expected that the resulting hydrodynamic forces on the SSP are greatest in this state. As seen in Figure 27 and Figure 28, the surge, heave forces, and pitch moments exerted on the SSP are notably higher for SS3 compared to other sea states. This is because the larger wave amplitudes and longer periods associated with SS3 generate stronger interactions between the waves and the platform, leading to increased forces and moments.

In particular, the heaving forces are plotted with negative values in the figures, reflecting the fact that these forces are measured at the centre of mass of the platform, which is located below the SWL. The negative sign indicates the downward direction of the forces relative to the SWL. Despite the significant wave heights and energy in SS3, the SSP's vertical displacement in heave motion stabilizes after the initial transient phase. Following the initial displacement, the variation in the heave motion remains within 1 meter, even for SS3. This indicates that the SSP's design effectively dampens large vertical movements, maintaining stability in extreme sea states.

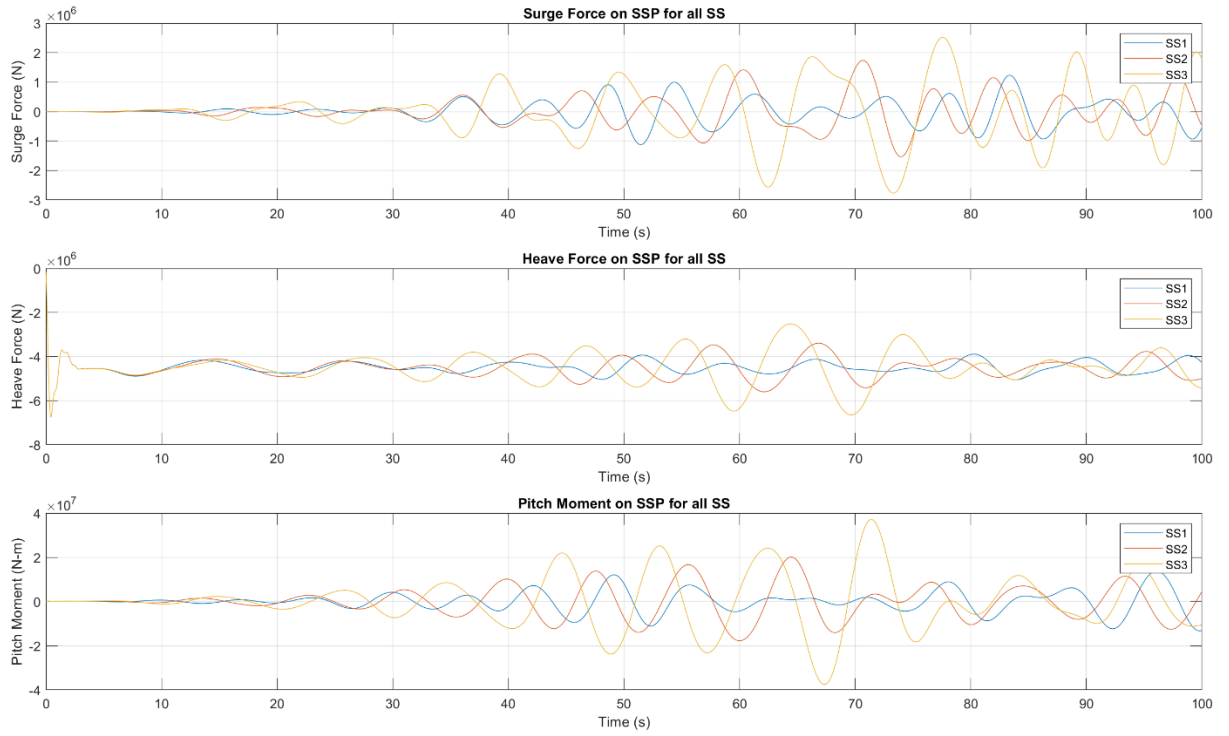


Figure 27. Forces and moment acting on SSP for different SS

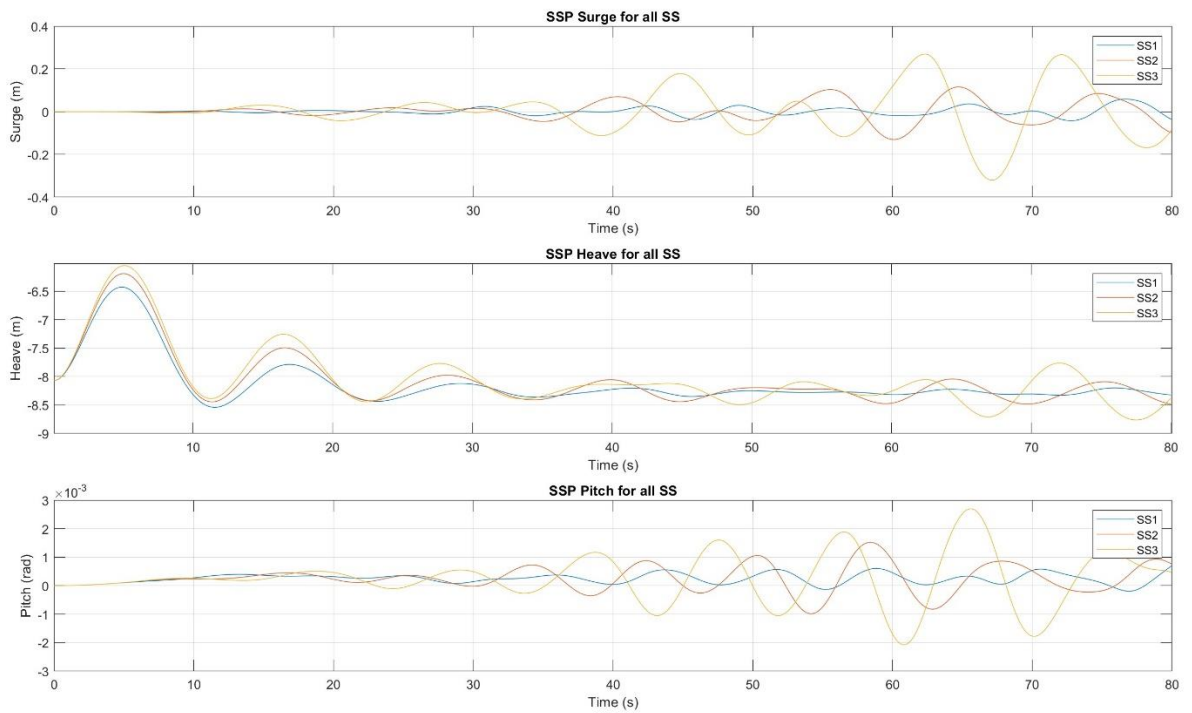


Figure 28. SSP surge, heave and pitch for different SS

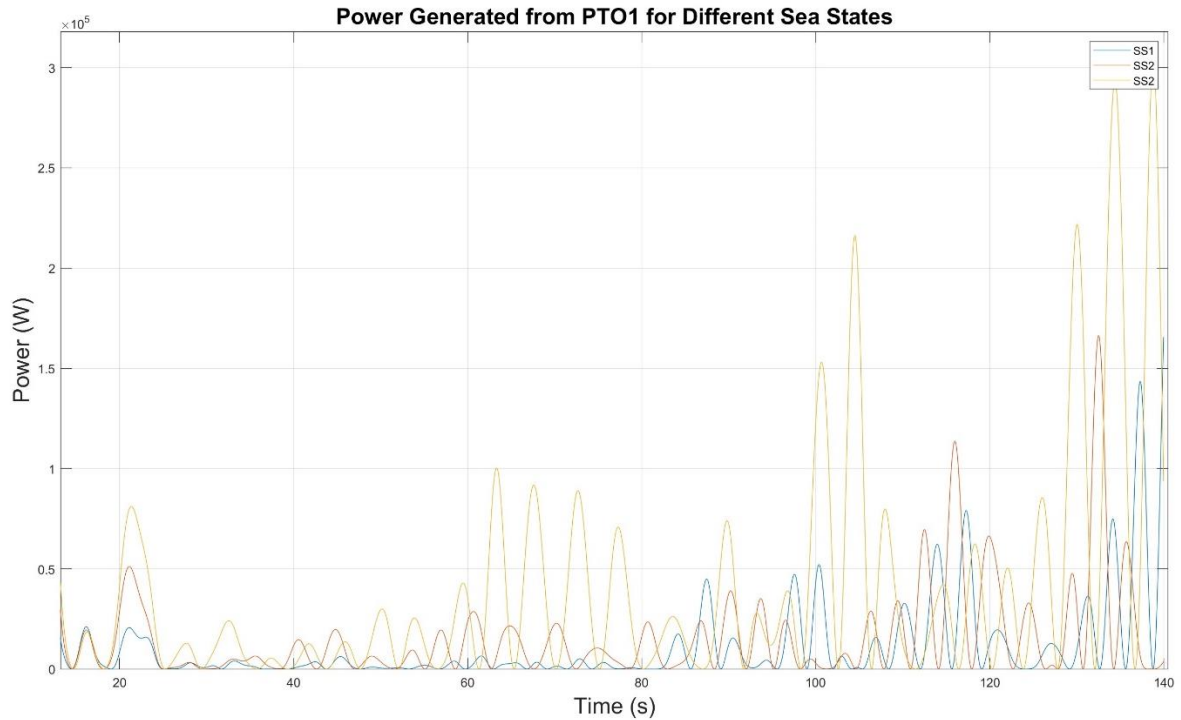


Figure 29. Power generation from WEC 1 for different SS

Figure 29. shows the power generation from WEC 1. The graph demonstrates the potential for significant power generation from wave energy, even under moderate sea states. The variation in the power and forces validate the dynamic behaviour of the WECs. Despite the fluctuations, WEC 1 demonstrates the ability to generate significant amounts of power, particularly in more energetic waves. This indicates that even in moderate sea states, where the wave energy is lower than in more extreme conditions, WEC 1 is capable of consistently capturing and converting wave energy into usable power.

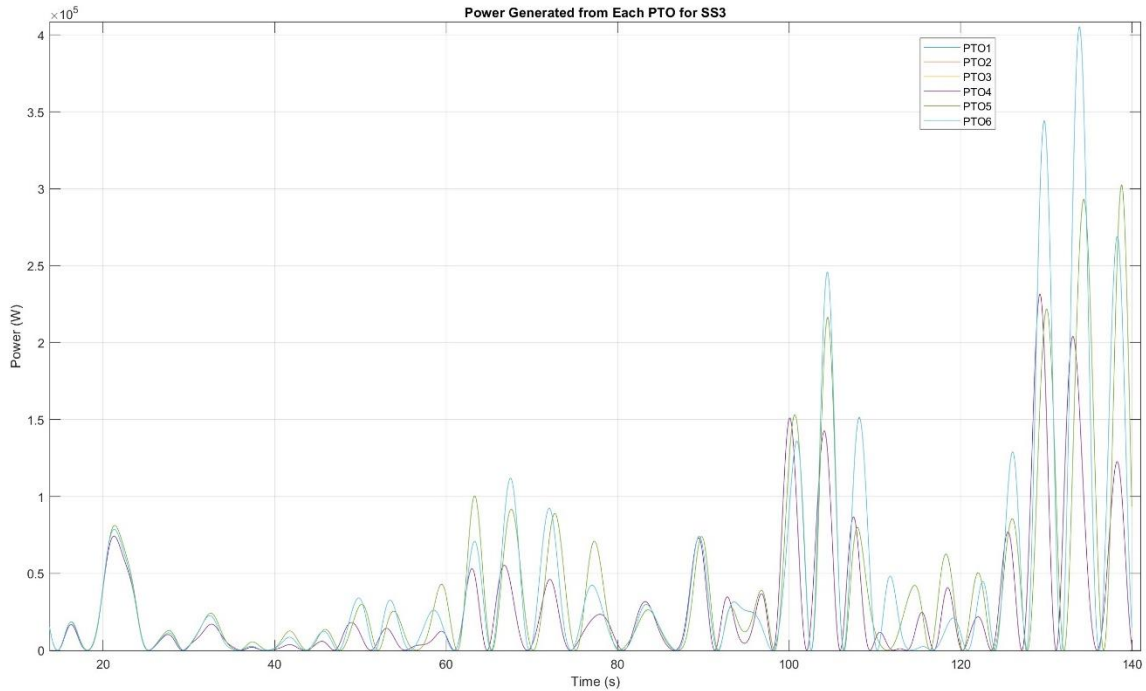


Figure 30. Power generated by each WEC for SS3

In Figure 30., the power generation capabilities of each WEC are plotted, highlighting how the layout of the WECs impacts their energy capture. WECs 1, 5, and 6 consistently produce higher power output compared to the others. This can be attributed to their position within the array, as shown in Figure 14., where WECs 1 and 6 are located at the outermost edges, directly facing the incoming waves. These positions allow them to absorb the most energy from the wave front, leading to enhanced power generation. WEC 5, positioned centrally, also benefits from the surrounding wave interactions, further increasing its output. This analysis underscores the importance of WEC array positioning in maximizing energy capture efficiency.

5. Conclusion

The conclusion summarizes the major findings of the study, emphasizing the potential of hybrid floating platforms for renewable energy generation. It reflects on the implications of the research, particularly regarding the stability and efficiency of such systems in offshore environments. The conclusion also outlines possible future research directions, including the exploration of economic feasibility and additional experimental validations.

The overall purpose of this study was to understand the ongoing development in the field of ocean renewable energy sector and contribute to its research. This work can be considered a part of the exploration going on for hybrid wind and wave systems. As mentioned in section 1.3, the two main objectives were to understand the impact of the integration of WECs with SSP in terms of stability and power generation. This was done using a combination of frequency domain and time domain analysis. The methodology

explicitly mentions the detailed steps taken to numerically model the HWWFP system. The conclusion of the study is as follows:

- While both the SSP and the HFFWP exhibit similar surge and heave responses at higher frequencies, the HFFWP demonstrates improved pitch damping, suggesting that the WECs effectively reduce rotational motion. The platform's natural frequency for heave is evident in its pronounced heave motion at lower frequencies.
- The results of radiation damping for the hybrid wind-wave platform show that the addition of WECs has a positive impact on its hydrodynamic behaviour. While the surge damping is similar for both the SSP and the HFFWP at lower frequencies, the HFFWP exhibits higher surge damping at higher frequencies. In terms of heave and pitch damping, the HFFWP consistently demonstrates higher values compared to the SSP, indicating that the WECs contribute to improved platform stability and control.
- While the overall diffraction forces decrease with increasing frequency for both systems, the HFFWP consistently experiences higher forces, particularly in the surge and heave directions. The pitch diffraction force for the HFFWP is slightly lower at higher frequencies compared to the SSP. This suggests that the WECs may have a beneficial effect on reducing the platform's rotational motion.
- Along with the response analysis, it is important to note that planning the layout of the WECs also has a significant impact on the power generation capabilities. These findings validate the importance of optimal WEC placement in maximizing power generation, as supported by the data in reference [70].

6. Limitations and recommended future works

The study primarily focused on short-term hydrodynamic performance and power generation efficiency. The study evaluated the platform's performance under a limited range of sea states, primarily focusing on moderate wave conditions. Extreme conditions, such as those encountered during storms or hurricanes, were not explored. This limits the understanding of the platform's robustness and survivability under more challenging conditions. Simulations should be expanded to include extreme sea states, such as those experienced during storms and rogue waves. Understanding the platform's behaviour in such conditions will help improve its resilience and guide the design of fail-safe mechanisms to protect the structure under adverse conditions. Experimental testing in wave basins with scale models is also recommended to validate these simulations. Deploying prototypes in offshore environments would provide valuable data on platform stability, energy generation, and maintenance needs. Such trials would also reveal practical

challenges and opportunities for further technological improvements, accelerating the path toward commercial deployment.

Acknowledgements

To my parents and Riya, your steadfast support throughout these past years has been the foundation of my academic journey. Your faith in me and your ongoing encouragement have been priceless, and for that, I am truly thankful.

I would also like to express my sincere appreciation to my supervisor, Oriol Gomis-Bellmunt, for his invaluable guidance.

Finally, to my friends, your unwavering support and frequent check-ins have been a source of strength during the most challenging moments. Your encouragement has been invaluable.

To each of you, I offer my heartfelt thanks.

References

- [1] F. Z. Rebecca Williams, "GLOBAL OFFSHORE WIND REPORT 2023," GLOBAL WIND ENERGY COUNCIL, 28 August 2023 2023.
- [2] IRENA, "Floating offshore wind outlook," International Renewable Energy Agency, Abu Dhabi, 2024.
- [3] V. Masterson, "Wave energy: can ocean power solve the global energy crisis?," March 22, 2022.
- [4] A. Felix *et al.*, "Wave Energy in Tropical Regions: Deployment Challenges, Environmental and Social Perspectives," *Journal of Marine Science and Engineering*, vol. 7, no. 7, p. 219, 2019. [Online]. Available: <https://www.mdpi.com/2077-1312/7/7/219>.
- [5] R. Pelc, "Renewable energy from the ocean," *Marine Policy*, 2002 2002, doi: [https://doi.org/10.1016/S0308-597X\(02\)00045-3](https://doi.org/10.1016/S0308-597X(02)00045-3).
- [6] S. H. Salter, "Wave power," *Nature*, vol. 249, no. 5459, pp. 720-724, 1974/06/01 1974, doi: 10.1038/249720a0.
- [7] A. Myhr, C. Bjerkseter, A. Ågotnes, and T. A. Nygaard, "Levelised cost of energy for offshore floating wind turbines in a life cycle perspective," *Renewable energy*, vol. 66, pp. 714-728, 2014.
- [8] D. Roddier, C. Cermelli, A. Aubault, and A. Weinstein, "WindFloat: A floating foundation for offshore wind turbines," *Journal of renewable and sustainable energy*, vol. 2, no. 3, 2010.
- [9] C. M. Wang, T. Utsunomiya, S. C. Wee, and Y. S. Choo, "Research on floating wind turbines: a literature survey," *The IES Journal Part A: Civil & Structural Engineering*, vol. 3, no. 4, pp. 267-277, 2010/11/01 2010, doi: 10.1080/19373260.2010.517395.
- [10] H. R. Ghafari, A. Neisi, H. Ghassemi, and M. Iranmanesh, "Power production of the hybrid Wavestar point absorber mounted around the Hywind spar platform and its dynamic response," *Journal of Renewable and Sustainable Energy*, vol. 13, no. 3, 2021, doi: 10.1063/5.0046590.
- [11] J. S. Rony and D. Karmakar, "Coupled Dynamic Analysis of Hybrid Offshore Wind Turbine and Wave Energy Converter," *Journal of Offshore Mechanics and Arctic Engineering*, vol. 144, no. 3, 2021, doi: 10.1115/1.4052936.
- [12] J. S. Rony and D. Karmakar, "Coupled dynamic analysis of hybrid STLP-WEC offshore floating wind turbine with different mooring configurations," *Journal of Ocean Engineering and Marine Energy*, vol. 9, no. 4, pp. 623-651, 2023/11/01 2023, doi: 10.1007/s40722-023-00287-w.
- [13] L. Castro-Santos, E. Martins, and C. Guedes Soares, "Cost assessment methodology for combined wind and wave floating offshore renewable energy systems," *Renewable Energy*, vol. 97, pp. 866-880, 2016/11/01/ 2016, doi: <https://doi.org/10.1016/j.renene.2016.06.016>.
- [14] A. H. Slocum, J. M. Kluger, and S. Mannai, "Energy Harvesting and Storage System Stabilized Offshore Wind Turbines," *2019 Offshore Energy and Storage Summit (OSES)*, pp. 1-6, 2019.
- [15] J. J. A. Robertson, F. Wendt, A. Goupee, H. Dagher, "Definition of the OC5 DeepCwind Semisubmersible Floating System " NREL, 2013.
- [16] D. O'Donnell, J. Murphy, and V. Pakrashi, "Comparison of Response Amplitude Operator Curve Generation Methods for Scaled Floating Renewable Energy Platforms in Ocean Wave Basin," *ASME Letters in Dynamic Systems and Control*, vol. 1, no. 2, 2020, doi: 10.1115/1.4049169.

- [17] J. Bosboom, *Oscillations of the ocean water surface*. Delft University of Technology, 2021.
- [18] "Ansys Theory Manual." Ansys https://ansyshelp.ansys.com/public/account/secured?returnurl=/Views/Secured/corp/v242/en/aqwa_thy/aqwa_thy.html (accessed July 26, 2024).
- [19] B. Guo and J. V. Ringwood, "Geometric optimisation of wave energy conversion devices: A survey," *Applied Energy*, vol. 297, p. 117100, 2021/09/01/ 2021, doi: <https://doi.org/10.1016/j.apenergy.2021.117100>.
- [20] A. H. Techet, 2005.
- [21] L. S. Sugar, "PERFORMANCE OF A NEAR SHORE OSCILLATING WAVE SURGE CONVERTER WITH VARIABLE FLAP CONFIGURATIONS " Master of Science in Mechanical Engineering, Department of Engineering East Carolina University 2021.
- [22] D. Apsley, "Waves: Linear Wave Theory," *Hydraulics*, 2024. [Online]. Available: <https://personalpages.manchester.ac.uk/staff/david.d.apsley/lectures/hydraulics3/WavesLinear.pdf>
- [23] Falnes, J , Author and Perlin, M , Reviewer, "Ocean Waves and Oscillating Systems: Linear Interactions Including Wave-Energy Extraction," *Applied Mechanics Reviews*, vol. 56, no. 1, pp. B3-B3, 2003, doi: 10.1115/1.1523355.
- [24] "INNOVATION OUTLOOK OCEAN ENERGY TECHNOLOGIES," IRENA, 2020. [Online]. Available: https://www.irena.org/-/media/Files/IRENA/Agency/Publication/2020/Dec/IRENA_Innovation_Outlook_Ocean_Energy_2020.pdf
- [25] "Offshore renewables: An action agenda for deployment, International Renewable Energy Agency," IRENA, Abu Dhabi, 2021. [Online]. Available: [/-/media/Files/IRENA/Agency/Publication/2021/Jul/IRENA_G20_Offshore_renewables_2021.pdf](https://www.irena.org/-/media/Files/IRENA/Agency/Publication/2021/Jul/IRENA_G20_Offshore_renewables_2021.pdf)
- [26] "Boosting Offshore Renewable Energy for a Climate Neutral Europe," ed. Brussels: European Commission, 2020.
- [27] D. Magagna, R. Monfardini, and A. Uihlein, "Ocean energy in Europe," *International Marine Energy Journal*, vol. 1, pp. 1-7, 08/30 2018, doi: 10.36688/imej.1.1-7.
- [28] R. W. Ricardo, "NSOG_non-binding_offshore_goals_final." [Online]. Available: <https://circabc.europa.eu/ui/group/8f5f9424-a7ef-4dbf-b914-1af1d12ff5d2/library/5dbd6168-e529-4604-a4d0-6c2c7cfb4b62/details>
- [29] "Vindeby Offshore Wind Farm." [Online]. Available: <https://tethys.pnnl.gov/wind-project-sites/vindeby-offshore-wind-farm#description>
- [30] V. N. Dinh and B. Basu, "On the modeling of spar-type floating offshore wind turbines," *Key Engineering Materials*, vol. 569, pp. 636-643, 2013.
- [31] I. IEA, "Energy technology perspectives 2017," *Catalysing Energy Technology Transformations*, 2017.
- [32] C. L. Archer and M. Z. Jacobson, "Evaluation of global wind power," *Journal of Geophysical Research: Atmospheres*, vol. 110, no. D12, 2005.
- [33] T. Asim, S. Z. Islam, A. Hemmati, and M. S. U. Khalid, "A Review of Recent Advancements in Offshore Wind Turbine Technology," *Energies*, vol. 15, no. 2, p. 579, 2022. [Online]. Available: <https://www.mdpi.com/1996-1073/15/2/579>.
- [34] M. Karimirad, *Offshore Energy Structures*: Springer Cham, 2014.
- [35] "Fukushima Floating Offshore Wind Farm Demonstration Project." [Online]. Available: <https://www.fukushima-forward.jp/english/>
- [36] "Hywind Scotland." [Online]. Available: <https://www.equinor.com/energy/hywind-scotland>
- [37] "WindFloat Atlantic." <https://www.windfloat-atlantic.com/the-wind-farm/#project> (accessed).

- [38] O. Ishchuk, "Problems of Floating offshore wind plants verification according to industry standards." [Online]. Available: <https://sdcoverifier.com/articles/problems-of-floating-offshore-wind-plants-verification-according-to-industry-standards/>
- [39] F. Ahmad, *Design of Floating Offshore Platform*. 2021.
- [40] "Wind Float T." Principle Power. <https://www.principlepower.com/windfloatt> (accessed.
- [41] "PivotBuoy Project: part-scale prototype in the Canary Islands." X1 Wind. <https://www.x1wind.com/projects/pivotbuoy-project-part-scale-prototype-in-the-canary-islands/> (accessed.
- [42] "Sustainable offshore solutions." Ocergy. <https://www.ocergy.com/ocg-wind#:~:text=The%20OCG%2DWind%20is%20a%20four%2Dcolumn%20semi%2Dsubmersible,designed%20for%20large%20wind%20turbines.> (accessed.
- [43] DeepCwind. <https://www.deepcwindco.com/> (accessed.
- [44] Robertson, "Summary of Conclusions and Recommendations Drawn From the DeepCwind Scaled Floating Offshore Wind System Test Campaign," *ASME 2013 32nd International Conference on Ocean, Offshore and Arctic Engineering*, 2013, doi: 10.1115/OMAE2013-10817.
- [45] T. P. Mazarakos and S. A. Mavrakos, "Wave-Current Interaction Effects on the OC4 DeepCwind Semi-Submersible Floating Offshore Wind Turbine," *Journal of Marine Science and Engineering*, vol. 12, no. 9, p. 1509, 2024. [Online]. Available: <https://www.mdpi.com/2077-1312/12/9/1509>.
- [46] G. M. Stewart, M. A. Lackner, A. Robertson, J. Jonkman, and A. J. Goupee, "Calibration and Validation of a Fast Floating Wind Turbine Model of the Deepcwind Scaled Tension-Leg Platform," presented at the Conference: Proceedings of the Twenty-Second International Offshore and Polar Engineering Conference (ISOPE-2012), 17-22 June 2012, Rhodes, Greece; Related Information: See CP-5000-54822 for preprint, United States, 2012. [Online]. Available: <https://www.osti.gov/biblio/1054419>.
- [47] W. Wang, S. Fan, Y. You, C. Zhao, L. Xu, and G. Wang, "Numerical and Experimental Study on an Anti-Oscillation Device for the DeepCwind Floating Semi-Submersible Turbine Platform," *Energies*, vol. 16, no. 3, p. 1034, 2023. [Online]. Available: <https://www.mdpi.com/1996-1073/16/3/1034>.
- [48] B. Drew, A. R. Plummer, and M. N. Sahinkaya, "A review of wave energy converter technology," ed: Sage Publications Sage UK: London, England, 2009.
- [49] A. F. d. O. Falcão, "Wave energy utilization: A review of the technologies," *Renewable and sustainable energy reviews*, vol. 14, no. 3, pp. 899-918, 2010.
- [50] T. W. Thorpe, "A brief review of wave energy," 1999.
- [51] Corpower. "CorPower Technology." <https://corpowersocean.com/> (accessed 2024).
- [52] "SEABASED " <https://seabased.com/the-technology> (accessed.
- [53] D. Curto, V. Franzitta, and A. Guercio, "Sea wave energy. A review of the current technologies and perspectives," *Energies*, vol. 14, no. 20, p. 6604, 2021.
- [54] D. Valério, M. J. Mendes, P. Beirão, and J. S. da Costa, "Identification and control of the AWS using neural network models," *Applied Ocean Research*, vol. 30, no. 3, pp. 178-188, 2008.
- [55] K. Tarrant and C. Meskell, "Investigation on parametrically excited motions of point absorbers in regular waves," *Ocean Engineering*, vol. 111, pp. 67-81, 2016.
- [56] Y. Liu, Y. Li, F. He, and H. Wang, "Comparison study of tidal stream and wave energy technology development between China and some Western Countries," *Renewable and Sustainable Energy Reviews*, vol. 76, pp. 701-716, 2017.
- [57] B. Guo, T. Wang, S. Jin, S. Duan, K. Yang, and Y. Zhao, "A Review of Point Absorber Wave Energy Converters," *Journal of Marine Science and Engineering*, vol. 10, no. 10, p. 1534, 2022. [Online]. Available: <https://www.mdpi.com/2077-1312/10/10/1534>.

- [58] E. Edwards, "Optimization of the Geometry of Axisymmetric Point-absorber Wave Energy Converters," Doctor of Philosophy in Mechanical Engineering, Department of Mechanical Engineering, MASSACHUSETTS INSTITUTE OF TECHNOLOGY, 2020. [Online]. Available: <http://dspace.mit.edu/handle/1721.1/7582>
- [59] Y. Wang, W. Shi, C. Michailides, L. Wan, H. Kim, and X. Li, "WEC shape effect on the motion response and power performance of a combined wind-wave energy converter," *Ocean Engineering*, vol. 250, p. 111038, 2022/04/15/ 2022, doi: <https://doi.org/10.1016/j.oceaneng.2022.111038>.
- [60] M. J. Muliawan, M. Karimirad, and T. Moan, "Dynamic response and power performance of a combined Spar-type floating wind turbine and coaxial floating wave energy converter," *Renewable Energy*, vol. 50, pp. 47-57, 2013/02/01/ 2013, doi: <https://doi.org/10.1016/j.renene.2012.05.025>.
- [61] J. Hu et al., "Optimal design and performance analysis of a hybrid system combining a floating wind platform and wave energy converters," *Applied Energy*, vol. 269, p. 114998, 2020/07/01/ 2020, doi: <https://doi.org/10.1016/j.apenergy.2020.114998>.
- [62] B. Wang et al., "The Energy Conversion and Coupling Technologies of Hybrid Wind-Wave Power Generation Systems: A Technological Review," *Energies*, vol. 17, no. 8, p. 1853, 2024. [Online]. Available: <https://www.mdpi.com/1996-1073/17/8/1853>.
- [63] Z. Gao et al., "D4. 6-Synthesis-Modelling and Testing: Methodology and Validation," *EU FP7 MARINA Platform Project. NTNU*, 2014.
- [64] L. Wan, Z. Gao, T. Moan, and C. Lugni, "Experimental and numerical comparisons of hydrodynamic responses for a combined wind and wave energy converter concept under operational conditions," *Renewable Energy*, vol. 93, pp. 87-100, 2016/08/01/ 2016, doi: <https://doi.org/10.1016/j.renene.2016.01.087>.
- [65] C. Michailides, Z. Gao, and T. Moan, "Experimental study of the functionality of a semisubmersible wind turbine combined with flap-type Wave Energy Converters," *Renewable Energy*, vol. 93, pp. 675-690, 2016/08/01/ 2016, doi: <https://doi.org/10.1016/j.renene.2016.03.024>.
- [66] "Copernicus Marine Service." Copernicus. <https://marine.copernicus.eu/about> (accessed).
- [67] "Global Ocean Waves Reanalysis," ed.
- [68] J. V. Ringwood, G. Bacelli, and F. Fusco, "Energy-Maximizing Control of Wave-Energy Converters: The Development of Control System Technology to Optimize Their Operation," *IEEE Control Systems*, vol. 34, pp. 30-55, 2014.
- [69] U.-J. Lee, W.-M. Jeong, and H.-Y. Cho, "Estimation and Analysis of JONSWAP Spectrum Parameter Using Observed Data around Korean Coast," *Journal of Marine Science and Engineering*, vol. 10, no. 5, p. 578, 2022. [Online]. Available: <https://www.mdpi.com/2077-1312/10/5/578>.
- [70] M. J. Lawson, Y.-H. Yu, K. Ruehl, and C. Michelen, "Development and Demonstration of The WEC-Sim Wave Energy Converter Simulation Tool," 2014.

Appendix A

To run a simulation in WEC-Sim, you need hydrodynamic coefficients from Aqwa in .h5 format calculated at the centre of gravity (COG), SolidWorks geometry files in .STL format, a Simulink model that includes a global reference frame, various bodies, PTOs, and constraints, and a properly populated WEC-Sim input file code.

WEC-sim reads the hydrodynamic data in .h5 format. Hence, the data obtained from AQWA is converted from .AH1 and .LIS to .h5 format using the bemio.m script. Here, ANALYSIS to is the file generated by AQWA.

```
hydro = struct();  
hydro = readAQWA(hydro, 'ANALYSIS.AH1', 'ANALYSIS.LIS');  
hydro = radiationIRF(hydro,100,[],[],[],[]);  
hydro = radiationIRFSS(hydro,[],[]);  
hydro = excitationIRF(hydro,100,[],[],[],[]);  
writeBEMIOH5(hydro)
```

STL format of the CAD is into the case directory. It is important to note that all the input files must be in the same case directory for WEC-sim to run.

A Simulink model needs to be created which represents the assembly of the HWWFP system. This also includes constraints and PTOs. As seen in figure 26. a total of 7 rigid body blocks are input in the model. Body(1) is the SSP and bodies(2-7) are the WECs. A global reference frame block is added, which is a crucial component that defines the global coordinates and various simulation settings. It acts as the reference point for the entire simulation, essentially representing the seabed. The SSP is connected to the global reference frame (yellow block) through a constraint. The 6 WECs are connected between the SSP and constraint, through translational PTOs.

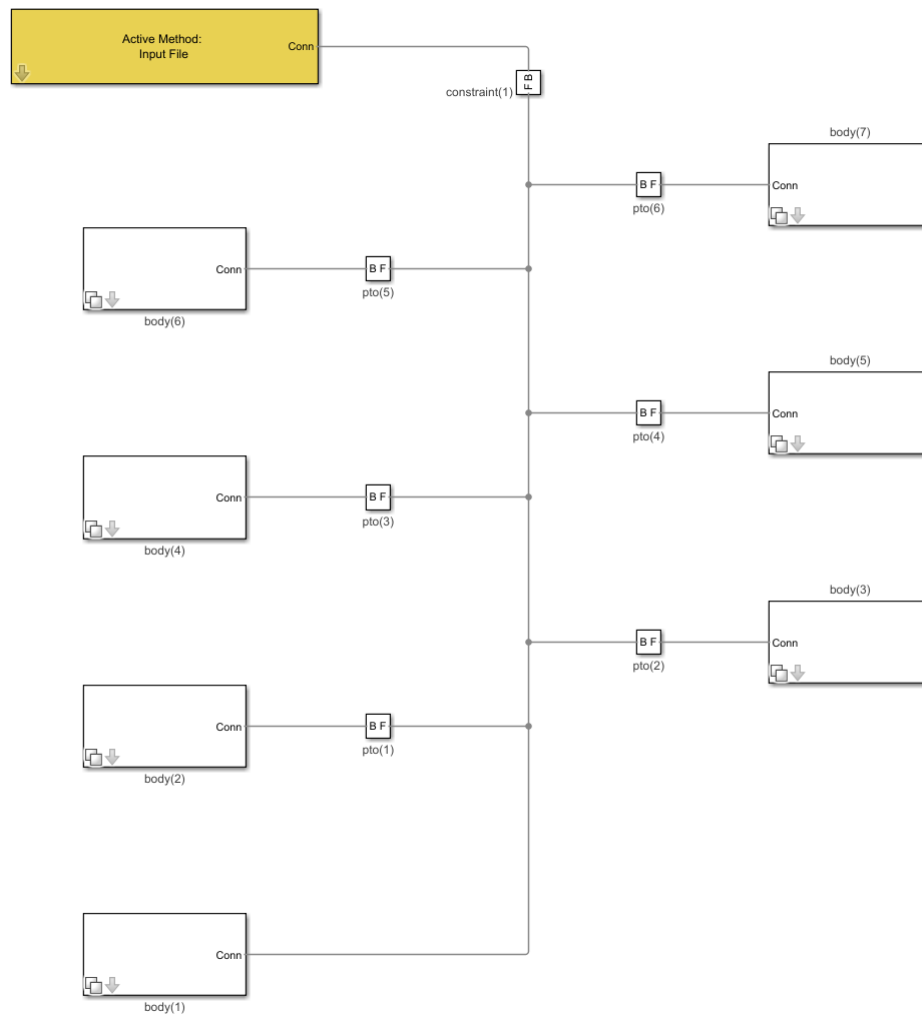


Figure 31. HWWFP Simulink model

A single input file stores all this data in WEC-sim, it is the `wecSimInputFile.m`. All of the simulation data and parameters are needed to be defined in this file. The script for SS1 can be seen below.

Simulation data

```
simu = simulationClass();
simu.simMechanicsFile = 'HWWFP.slx';
simu.mode = 'normal';
simu.explorer = 'off';
simu.startTime = 0;
simu.rampTime = 150;
simu.endTime = 180;
simu.solver = 'ode4';
simu.dt = 0.05;
```

Wave class

```
waves = waveClass('irregular');
```

```
waves.height = 2.5;  
waves.period = 9;  
waves.spectrumType = 'JS';  
waves.bem.option = 'EqualEnergy';  
waves.phaseSeed = 1;
```

Body data

SSP

```
body(1) = bodyClass('ANALYSIS.h5');  
body(1).geometryFile = 'SSP.stl';  
body(1).mass = 13958000;  
body(1).inertia = [13947000000 15552000000 13692000000];
```

WECs

```
body(2) = bodyClass('ANALYSIS.h5');  
body(2).geometryFile = 'PAWEC.stl';  
body(2).mass = 17700;  
body(2).inertia = [312924.78 314084.35 316647.54];
```

```
body(3) = bodyClass('ANALYSIS.h5');  
body(3).geometryFile = 'PAWEC.stl';  
body(3).mass = 17700;  
body(3).inertia = [312924.78 314084.35 316647.54];
```

```
body(4) = bodyClass('ANALYSIS.h5');  
body(4).geometryFile = 'PAWEC.stl';  
body(4).mass = 17700;  
body(4).inertia = [312924.78 314084.35 316647.54];
```

```
body(5) = bodyClass('ANALYSIS.h5');  
body(5).geometryFile = 'PAWEC.stl';  
body(5).mass = 17700;  
body(5).inertia = [312924.78 314084.35 316647.54];
```

```
body(6) = bodyClass('ANALYSIS.h5');  
body(6).geometryFile = 'PAWEC.stl';  
body(6).mass = 17700;  
body(6).inertia = [312924.78 314084.35 316647.54];
```

```
body(7) = bodyClass('ANALYSIS.h5');  
body(7).geometryFile = 'PAWEC.stl';  
body(7).mass = 17700;  
body(7).inertia = [312924.78 314084.35 316647.54];
```

PTO and constraints

```
constraint(1) = constraintClass('Constraint1');  
constraint(1).location = [0 0 0];
```

```
pto(1) = ptoClass('PTO1');  
pto(1).stiffness = 0;  
pto(1).damping = 2806006.192;  
pto(1).location = [-14.579 -8.2498 -3];
```



```
pto(2) = ptoClass('PT01');
pto(2).stiffness = 0;
pto(2).damping = 2806006.192;
pto(2).location = [0.14 -16.75 -3];

pto(3) = ptoClass('PT01');
pto(3).stiffness = 0;
pto(3).damping = 2806006.192;
pto(3).location = [14.44 8.5 -3];

pto(4) = ptoClass('PT01');
pto(4).stiffness = 0;
pto(4).damping = 2806006.192;
pto(4).location = [14.44 -8.5 -3];

pto(5) = ptoClass('PT01');
pto(5).stiffness = 0;
pto(5).damping = 2806006.192;
pto(5).location = [-14.518 8.25 -3];

pto(6) = ptoClass('PT01');
pto(6).stiffness = 0;
pto(6).damping = 2806006.192;
pto(6).location = [0.14 16.75 -3];
```